CLM-P 675

UKAEA

Preprint

LASER DIAGNOSTICS IN CONTROLLED THERMONUCLEAR FUSION

D. E. EVANS

CULHAM LABORATORY
Abingdon Oxfordshire

1982

CLM-P 675

LASER DIAGNOSTICS IN CONTROLLED THERMONUCLEAR FUSION

D.E. Evans
Culham Laboratory, Abingdon, Oxon. OX14 3DB, England
(Euratom/UKAEA Fusion Association)

(To be published by Academic Press, New York,
in Applied Atomic Collision Physics, Vol.II,
Part I Controlled Thermonuclear Fusion, Chapter VI)

June 1982

C O N T E N T S

1. INTRODUCTION

All diagnostic methods based on transmitting electromagnetic radiation through plasma depend on a degree of coherence in the probing beam. The early availability of quasi-coherent microwave sources made possible the extensive development of interferometry, Faraday rotation measurements, and turbulence scattering in the cm and mm wavebands. The coherence requirement is likewise responsible for the failure to extend these techniques to shorter wavelengths by the use of thermal sources. Indeed, the need to increase the range of plasmas accessible to investigation by reducing the probing wavelength could be met only when lasers became obtainable after 1960.

The appropriate way to describe the propagation of a beam of coherent radiation is by gaussian optics (Siegman 1971) and a complete account of its interaction with plasma, including scattering by the electrons, is given in terms of phase shifts, by refraction theory.

Plasma with magnetic field behaves as a birefringent, optically active medium, propagation perpendicular to the field being purely birefringent, propagation parallel to it, purely optically active. It can be shown (Ramachandran and Ramaseshan, 1961) that for any direction of propagation there exist two characteristic waves with different phase velocities whose state of polarization remains unchanged during propagation, and the characteristic polarizations are orthogonal. A beam propagating in arbitrary direction can be resolved into two characteristic components, which will travel at different phase velocities determined by the corresponding characteristic refractive indexes, then recombine to produce an altered polarization and phase relative to a second beam that traversed the same distance of empty space. This is the basis of the Faraday rotation method for measuring magnetic field, and of interferometry designed to measure plasma electron density. It is also, though less obviously, the process underlying Thomson scattering. The present article is devoted to a short account of these three topics.

2. FARADAY ROTATION

2.(i) Refraction and the Poincare Sphere

Faraday rotation can conveniently be discussed with reference to the Poincare unit sphere (Ramachandran and Ramaseshan, 1961; Born and Wolf, 1964), points on whose surface can be made to correspond to all possible states of optical polarization in the following way. If the polarization of light propagating in the +z direction is specified by its ellipticity $\chi = \tan^{-1} b/a$, and by the angle ψ between the ellipse major axis and the x-coordinate axis, as shown in Figure 1, then (χ, ψ) defines a unique point having Cartesian coordinates (Stokes parameters)

$$\begin{aligned} S_x &= \cos 2\chi \cos 2\psi \\ S_y &= \cos 2\chi \sin 2\psi \\ S_z &= \sin 2\chi \end{aligned} \qquad \ldots(1)$$

on the surface of the unit sphere. It will be seen that orthogonal polarizations occupy diametrically opposite points on the sphere, with plane polarized light at the equator in the x-y plane, and left and right handed circularly polarized light at the north (+z) and south (-z) poles respectively. A line of longitude is the locus of all ellipses at the angle ψ , and a line of latitude that of all ellipses having a fixed shape (χ) but all orientations.

Being orthogonal, the two characteristic waves referred to in the Introduction define an axis through the sphere's centre, and it can be shown that evolution of polarization during propagation can be represented on the Poincare sphere by a rotation about this axis equal to a phase difference $\varphi = (\omega/c)\, L\, (\mu_1 - \mu_2)$, where ω is the optical angular frequency, c the velocity of light, L the geometric distance of propagation, and μ_1 and μ_2 are the characteristic refractive indexes. For a homogeneous medium, if $\underline{n}$ is unit vector in the direction of this axis of rotation, and $\underline{u}$, also a unit vector, defines the polarization of the incident light, the emergent polarization will be given by the vector

$$\underline{u}' = \underline{u} \cos \varphi + \underline{u}\cdot\underline{n}\, (1 - \cos \varphi)\, \underline{n} + (\, \underline{n} \times \underline{u}\,) \sin \varphi \qquad \ldots(2)$$

2.(ii) Characteristic Waves for Magnetised Plasma

Assuming the magnetic field B lies in the y-z plane at an angle θ to the direction of radiation propagation (+z), it can be shown that the characteristic waves are elliptically polarized with axes along the x and y coordinate axes, as shown in Figure 2.

De Marco and Segre (1972) introduce the parameter F, where

$$\frac{1}{F} = \frac{\Omega_c}{2(1-\Omega_p^2)} \frac{\sin^2\theta}{\cos\theta} , \qquad ...(3)$$

allowing one to write the Appleton-Hartree equation (Heald and Wharton, 1965) for the characteristic refractive indexes μ as

$$1-\mu^2 = \frac{\Omega_p^2}{1 \pm \frac{\Omega_{c_{\parallel}}}{F}[\sqrt{(1+F^2)} \mp 1]} . \qquad ...(4)$$

Here $\Omega_p \equiv \omega_{pe}/\omega$ and $\Omega_{c_{\parallel}} \equiv (\omega_{ce}/\omega)\cos\theta$, ω_{pe} and ω_{ce} being the electron plasma frequency and the electron gyrofrequency respectively.

The wave polarisation is (Heald and Wharton, 1965)

$$\tan\chi \equiv \frac{E_x}{E_y} = i\frac{\Omega_p^2 \mp (1-\mu^2)}{(1-\mu^2)\Omega_{c_{\parallel}}} = i\frac{\sqrt{(1+F^2)} \mp 1}{F} . \qquad ...(5)$$

That this turns out to be pure imaginary means that the phase difference between the x and y components is π/2, and the major axis of the ellipse lies in the x-direction (Born and Wolf p.29, 1964). The coordinates of the characteristic polarizations on the Poincare sphere are then determined by

$$\sin 2\chi = \mp\frac{F}{\sqrt{(1+F^2)}} , \quad \cos 2\chi = \frac{1}{\sqrt{(1+F^2)}} , \qquad ...(6)$$

and $\psi = \pi/2$ or 0 .

This has the general meaning that radiation passing through homogeneous magnetized plasma will alter its polarization both in ellipticity and in angular attitude of the plane of polarization. However it can be seen that if $F \gg 1$, the characteristic waves are almost right and left hand circularly polarized, and then the effect of the transit on polarization, represented by

rotation about the z-axis, is to leave the ellipticity unchanged while rotating the angle of the ellipse. In particular, radiation initially plane polarized experiences only a rotation of the plane of polarization, and this is popularly called Faraday rotation.

2.(iii) Faraday Effect as Rotation of Polarization

For $F \gg 1$ equation (4) above gives the indexes of refraction of the characteristic waves as

$$1-\mu^2 \approx \Omega_p^2 (1 \pm \Omega_{c_{\parallel}})^{-1} ,$$

and the angle Ψ/L through which the plane of polarization rotates per unit path length through the plasma becomes

$$\Psi/L = \varphi/2L = \tfrac{1}{2}\frac{\omega}{c}(\mu_1 - \mu_2) = \tfrac{1}{2}\frac{\omega}{c}\frac{\Omega_p^2 \Omega_{c_{\parallel}}}{1 - \Omega_{c_{\parallel}}} \approx \tfrac{1}{2}\frac{\omega}{c}\Omega_p^2 \Omega_{c_{\parallel}}$$

$$= 2.64 \times 10^{-13} \lambda^2 n_e B$$

provided $\Omega_{c_{\parallel}}^2 \ll 1$, λ is in cm, n_e in cm^{-3} and B in tesla.

It was pointed out by R W Wood (1967) that in the $F \gg 1$ approximation the effect of magnetic field on the dispersion curve, μ as a function of ω, is merely to shift its origin by an amount $\pm \frac{1}{2}\omega_{ce_{\parallel}}$, the Larmour frequency, but to leave its shape unchanged.

It cannot be taken for granted that the $F \gg 1$ condition, necessary for the foregoing simplification, will inevitably be met. For example, if a CD_3F laser (λ = 1.22 mm) is being used to measure Faraday rotation in a plasma with B = 3 tesla, F is already smaller than unity when θ is greater than 80° and an incident plane polarized wave will emerge with an elliptical component perpendicular to the incident plane of polarization which will be confused with the pure angular rotation of this plane.

To ensure the validity of the plane polarization approximation, the wavelength must be kept as small as possible, even though the Faraday rotation angle one seeks to measure is proportional to λ^2. Suppressing ellipticity has generally been held to be more important than a large rotation angle, however, and the measurement

of small rotations of the plane of polarization has accordingly been the subject of considerable experimental ingenuity. Two distinct approaches are in use. One relies on ratios of amplitudes, the other on phase shifts.

2.(iv) Amplitude Ratio Method: Half Shade Angle

A general description of the amplitude ratio method has been given by Falconer and Ramsden (1968). After traversing the plasma, the plane polarized probe beam of intensity I_o is divided into two equal parts by a polarization sensitive beam splitter. Each part meets a polarizer oriented $\frac{1}{2}\epsilon$ radians away from perpendicular to the initial polarization, as shown in Figure 3 . From polarimetry (Heller, 1960) $\frac{1}{2}\epsilon$ is termed the half-shade angle.

If the plane of polarization has experienced no rotation, the signal in each of the two channels will be $\frac{1}{2} I_o \sin^2 \frac{1}{2}\epsilon$, but a rotation θ will give rise to signals $I_\pm(\theta) = \frac{1}{2} I_o \sin^2(\frac{1}{2}\epsilon \pm \theta)$, and the ratio

$$R = \frac{I_+ - I_-}{I_+ + I_-} = \frac{\sin \epsilon \ \sin 2\theta}{1 - \cos \epsilon \cos 2\theta} ,$$

which is independent of the incident power I_o, will have a value between $\pm$ 1 . The sensitivity of this arrangement to small rotations is determined by the slope of the curve R as a function of θ near $\theta = 0$, viz.

$$\left.\frac{dR}{d\theta}\right|_{\theta=0} = \frac{2 \sin \epsilon}{1 - \cos \epsilon} .$$

One configuration sometimes adopted (Dougal et al, 1964 ; Brown et al, 1977) is to set the analysers at $\pm$ 45° to the incident plane of polarization, in which case R becomes simply $\sin 2\theta$ and $\left.\frac{dR}{d\theta}\right|_{\theta=0} = 2$.

A more sensitive configuration is one in which $\frac{1}{2}\epsilon$ is made less than 45°. When ϵ is small, the sensitivity of the ratio R to small changes in rotation becomes $\left.\frac{dR}{d\theta}\right|_{\theta=0} = 4/\epsilon$. Figure 4, displaying R as a function of rotation angle θ , shows that a choice of $\frac{1}{2}\epsilon$ smaller than

the expected value of θ would be foolish, and that the best choice of $\frac{1}{2}\varepsilon$ would be about twice the maximum rotation to be measured.

The minimum rotation θ that can be measured by this method is set ultimately by detector noise, but window birefringence, imperfections in the analysers, and simply the range of angles at which radiation impinges on the analysers may all be important limitations.

2.(v) Polarization Modulation Method

A quite different approach to small angle Faraday rotation measurement, involving modulating the incident radiation's polarization angle, was suggested by Kunz and Dodel (1978). The question of measuring poloidal field and its radial distribution in tokamak plasma by Faraday rotation has been extensively discussed (DeMarco and Segre 1972, Craig 1976, Segre 1978) and was successfully performed for the first time using this technique in the TFR plasma by Kunz and the TFR team (1978).

A disc of material transparent at the appropriate probe wavelength and with a reasonable Verdet constant is placed within a coil and located so that the plane polarized probe beam passes through it prior to encountering the plasma. For 337 μm radiation from an HCN laser, ferrite (Frayne 1968, Birch and Jones 1970) has been used, though a disc of suitable thickness absorbs about 80% of the incident power. A radio frequency current in the coil causes the plane of polarization to oscillate with an angular amplitude α of a few degrees. A detector, viewing the result through an analyser crossed with the initial polarization, produces a signal proportional to $I_o \sin^2(\alpha \sin \omega t) \approx \frac{1}{2} I_o \alpha^2 (1-\cos 2\omega t)$ for small α. Magnetized plasma in the path of the probe beam induces an additional rotation θ, resulting in a detector signal $I_o \sin^2(\theta + \alpha \sin \omega t)$ which is approximately $I_o [\theta^2 + \frac{1}{2}\alpha^2 (1 - \cos 2\omega t) + 2\alpha\theta \sin \omega t]$ for small α and θ. Comparison of this with the plasma-free expression above shows that the plasma contributes a term at the modulation frequency ω: $I_\omega = I_o 2\alpha\theta \sin \omega t$, and this can be

efficiently extracted from the detector output by the use of a lock-in amplifier referred to the radio frequency oscillator.

Assuming their experimental performance on TFR to be limited by detector NEP, Kunz et al (1978) expected a minimum measurable rotation of 0.6 mrad for a modulation frequency of 100 Hz and a GaAs detector. In practice they realized a minimum of about 1 mrad and ascribed the discrepancy to amplifier noise.

2.(vi) Amplitude Independent Polarization Modulation

Though very different from the half-shade angle technique, the method just described remains amplitude dependent, and its success depends on the constancy of the probe beam intensity. Any component of probe beam vibration at the modulation frequency will be wrongly attributed to plasma Faraday effect. Dodel and Kunz (1978) have suggested a modification that altogether removes the dependence on intensity, and converts the measurement to one of phase shift. The significant step is the replacement of the small amplitude oscillation imposed on the plane of polarization by a complete rotation through 2π. This is readily produced by superimposing right hand and left hand circularly polarized beams having a frequency difference $\Delta\omega$. The result is plane polarized radiation whose plane of polarization rotates at the frequency $\frac{1}{2}\Delta\omega$. Such a beam, viewed through an analyser by a square law detector, induces a signal component $\cos \Delta\omega t$. Plasma Faraday rotation appears as a phase shift resulting in $\cos(\Delta\omega t + \theta)$. Provided the frequency of rotation $\Delta\omega$ is chosen so that the condition $\left|\frac{2\pi}{\Delta\omega}\frac{d\theta}{dt}\right| < \pi$, θ can be deduced from the time shift between zero crossings of the signal with plasma relative to the signal without, in strict analogy with, and retaining all the advantages of the procedure introduced by Veron (1974) for interferometry.

Frequency shifts can be generated by the rotating grating method used by Veron, or by the detuning of a pair of optically pumped lasers, as demonstrated by Wolfe et al (1976).

3. INTERFEROMETRY

3.(i) Magnetic Field Independent Phase Shift

Interferometry is performed in laboratory plasmas to measure the electron density distribution, and is accordingly concerned with plasma refraction relative to free space, rather than the difference between characteristic wave refractive indexes as in Faraday rotation. Once again the choice of probe wavelength involves conflicting requirements. An interferometer measures phase difference $\Delta\varphi = 2\pi\lambda^{-1}L(1-\mu)$ and the use of short wavelength means μ will be well approximated by $1-\frac{1}{2}\Omega_p^2$, leading to the simple dependence $\Delta\varphi = r_e\lambda Ln_e$, r_e being the classical electron radius, n_e the electron density, and L the path length. But short wavelength also implies few fringes to measure.

On the other hand, while generating relatively many fringes, long wavelength entails the danger of gross refraction by density gradients, culminating in total opacity as the plasma frequency is approached. The choice of long wavelength can also invalidate convenient approximations for μ . Inspection of the Appleton-Hartree formula (equation 4) shows however that this can be avoided even at long wavelength provided the probe beam can be propagated as an ordinary mode ($\underline{E} \parallel \underline{B}$) perpendicular to the magnetic field $\underline{B}$, for then $\mu^2 = \mu_o^2 = 1-\Omega_p^2$ without approximation. In a tokamak where $\underline{B}$ is nearly toroidal and interferometer beams are confined to a minor cross-section, these conditions can readily be met.

Interferometers for studying magnetically confined plasmas have usually been assembled in the Mach-Zehnder or the Michelson configuration (Alpher and White, 1965 Jahoda and Sawyer 1971). A typical primitive layout would consist of a pair of beam splitters and a pair of mirrors as in Figure 5 . The first beam splitter divides a beam of coherent radiation from a laser into two channels, one of which passes through the plasma under investigation acquiring a phase shift $\varphi(t)$ relative to the other in the process. They then recombine on the

second beam splitter and are finally directed onto a square law detector giving rise to detection current $i \propto A \cos \varphi(t)$.

Extracting $\varphi(t)$ and hence the time history of the density from this detector current is complicated by the unwanted dependence on the amplitude A , which may itself be varying with time. It is further complicated by the ambiguity of the cosine function regarding the sign of its argument, which makes it impossible to distinguish increasing from decreasing φ , or to determine when a change in the sign of φ has occurred. Such an instrument will also be subject to spurious phase shifts due to vibration-induced variation in the optical path length. Remedies for the former failing have been sought in different forms of phase modulation technique, while vibration compensation arrangements have been invented to overcome the latter.

3.(ii) Phase Modulation: Zebra Stripe Interferometer

An elegant solution to these problems was demonstrated by Gibson and Reid (1964) who referred to their phase modulation technique as "zebra-striping" because of the appearance of the presentation on an oscilloscope. The scale of the problem of interpreting raw interference fringes can be judged from their confused appearance during a plasma discharge, shown in Figure 6. By contrast phase shift in units of $\frac{1}{2}\lambda$ can be read directly from the accompanying zebra stripe display. This gives an unambiguous indication of reversals in the changing optical path length, is entirely independent of fringe amplitude, and even lends itself to correction for vibration.

As applied to the three mirror interferometer of Ashby and Jephcott (1963), the method works by imposing controlled changes in the optical path length in the arm of the interferometer which will span the plasma. The mirror on that arm is caused to oscillate and the wave form driving the oscillator is shown on an oscilloscope. The interference fringes generated by the moving mirror are not themselves displayed, but instead are used to

modulate the oscilloscope brightness, one bright-up of the beam corresponding to each fringe maximum. The result is that the waveform appears discontinuous as though traced by a line of bright dashes, and because the fringes are caused by the waveform, the mth fringe always produces its bright-up at the same value of y-displacement. When the time base is run very slowly so as to show many cycles of the waveform on the screen at once, the bright dashes belonging to the mth fringe coalesce to form a horizontal stripe. A set of successive fringes thus appears on the oscilloscope screen as a pattern of horizontal stripes, whose spacing corresponds to the change in optical path length, $\frac{1}{2}\lambda$ in the Ashby-Jephcott arrangement, needed to go from one interference maximum to the next. This can be seen in Figure 6 .

Put quantitatively, the condition for an interference maximum or oscilloscope bright-up, is that the total optical path, consisting of the geometrical part L , the driven oscillation part $\ell_o(t)$, and the plasma contribution $\ell_p(t)$, be an integer multiple of $\frac{1}{2}\lambda$:

$$L + \ell_o(t) + \ell_p(t) = m\,(\tfrac{1}{2}\lambda) \ .$$

Now the oscilloscope displays the oscillation waveform

$$y = \text{const} \times \ell_o(t)$$

which becomes $y = \text{const} \times [m(\frac{1}{2}\lambda) - \ell_p(t) - L\,]$ for the locus of a fringe or a bright-up stripe. Here L is simply a constant displacement and may be tuned out and ignored.

Without plasma, the bright-up locus is $y = \text{const} \times [m(\frac{1}{2}\lambda)]$, a set of horizontal straight stripes whose spacing is proportional to $\frac{1}{2}\lambda$. With plasma, the displacement in the y-direction of each stripe follows faithfully the plasma's phase development in time, and the stripe spacing constitutes a calibrated scale against which the displacement can be measured in units of $\frac{1}{2}\lambda$. The maximum rate of change of phase that can be followed is one fringe per oscillation cycle of the mirror.

Sensitivity is determined by the smallest fraction of a fringe that can be detected. It could be increased

by the ratio of the wavelengths in a two laser modification of the system. A short wavelength would generate the calibration scale, and a long wavelength, traversing the same arrangement of mirrors, would produce the stripe whose displacement measures plasma phase shift.

Furthermore, a two wavelength scheme permits spurious vibration effects to be compensated. The expressions for the λ_1 stripe and the λ_2 stripe have as a common additive component the vibration-induced change in path length. The difference between such a pair of stripes is therefore vibration independent.

3.(iii) Phase Quadrature Interferometer: Optical

Another scheme that approaches the ambiguity problem in a different way is the quadrature interferometer, employing two signals out of phase with each other by 90°. Just as in the simple instrument the detector signal is $S = A \cos \varphi$, in the quadrature device, the two signals are $S_1 = A \cos \varphi$, and $S_2 = A \sin \varphi$, whose ratio, $S_2/S_1 = \tan \varphi$ is independent of the amplitude A. Unlike the simple system, therefore, this one is free from spurious influences such as refraction induced varying fringe contrast. Versions of the quadrature interferometer described by Heym (1968) and by Berger and Lovberg (1970) derived their two signals from separate portions of the beam aperture and could accordingly have been subject to misalignment uncertainty. Buchenauer and Jacobson (1977) avoid this danger by separating polarization components of the beam to obtain their signal pair.

Figure 7a diagrams the modified Mach-Zehnder arrangement proposed by Buchenauer and Jacobson. The laser beam is initially plane polarized, but a quarter wave plate in the reference arm converts this to circular polarization. Following the second beam splitter, a Wollaston prism analyses the circularly polarized reference into two mutually perpendicular plane polarized parts 90° out of phase, at the same time as it divides the plane polarized probe beam into two plane polarized but in-phase components. The four resulting beams are mixed in reference-plus-probe pairs on independent detectors, producing the signals

illustrated in Figure 7b. It can be seen that whenever one signal crosses its zero line the other is at an extremum, and in general, the amplitude $A = (S_1^2 + S_2^2)^{\frac{1}{2}}$ can be measured continuously throughout the plasma discharge, in contrast to what is possible in a simple interferometer. Moreover, the sign of $\frac{d\varphi}{dt}$ is at no point uncertain.

Finally it may be remarked that in the conventional instrument the uncertainty $\Delta\varphi$ in the determination of the phase shift is itself a function of φ , viz

$$\Delta\varphi = \Delta S / A \sin \varphi ,$$

and even diverges when φ is an integer multiple of π . In quadrature, by contrast, $\Delta\varphi_{rms} = \Delta S / A$, and is accordingly the same for all values of phase shift.

3.(iv) Phase Quadrature: Electrical Method

The quadrature technique is a powerful one and its extension to all probe beam wavelengths is desirable. But division of a beam of radiation into a pair of beams mutually orthogonal in phase can be accomplished optically only at wavelengths at which appropriate birefringent elements such as $\lambda/4$ plates and polarizing prisms are readily available. Universal applicability can be approached if the quadrature is performed electrically rather than optically, and this can be done provided an intermediate frequency is introduced at which electronics can operate with comfort.

Baker and Shu-Tso Lee (1979) obtained their intermediate frequency by Doppler shifting their probe beam frequency with a translating mirror on the Michelson arrangement on Doublet III . Another more versatile technique is to use Bragg diffraction by sound waves driven in some suitably transparent medium to induce a convenient frequency shift (Jacobson and Call, 1978, Hugenholtz and Meddens 1979) . The probe beam, carrying the plasma-induced phase shift $\cos(\omega t+\varphi)$, is mixed on the detector in the usual way, with the frequency shifted reference beam $\cos(\omega+\omega_B)t$ to generate a detector current only one component of which, $i_d \propto \cos(\omega_B t + \varphi)$ is at a frequency low enough to cause the electronics to

respond. A commercially available quadrature phase comparator can then be used to divide this current into two channels, one of which is subject to a $\pi/2$ phase shift relative to the other, before each is mixed with the Bragg cell driver waveform $\cos \omega_B t$. This yields currents in quadrature $i_1 = A \cos \varphi$ and $i_2 = A \sin \varphi$, in direct analogy with the optical quadrature signals of the Buchenauer and Jacobson apparatus.

3.(v) Vibration Compensated Quadrature Interferometer

Gowers and Lamb (1982) have used the principle just discussed to build a CO_2 laser quadrature interferometer for use in reverse field pinch plasmas, in which the intermediate frequency is 40 MHz , and incorporating a subsidiary common path HeNe laser interferometer for vibration compensation.

The experimental layout is essentially a Michelson configuration, as shown in Figure 8 . The 5 W 10.6 μm gaussian laser beam is divided in two by the Ge acousto-optic modulator (Bragg cell), and the undeviated zero order traverses the plasma twice before combining with the first order frequency-shifted reference beam on a liquid nitrogen cooled 100 MHz bandwidth CdHgTe infrared detector.

By coaxially aligning the zero and first order HeNe laser beams diffracted in a dense flint glass Bragg cell with the two 10.6 μm beams, and by using optical components compatible with both visible and IR wavelengths, i.e. ZnSe for beam splitters and Au-coated mirrors, a second simultaneously operating interferometer at 0.63 μm wavelength was formed. Using almost the same optical path for both visible and CO_2 interferometers allowed vibration occurring almost anywhere in the interferometer assembly to be compensated, since the shorter wavelength is relatively much less sensitive to plasma phase shifts, and much more sensitive to vibration than the longer wavelength. Figure 9 shows the quadrature waveforms obtained from the 10.6 μm system and also those from the visible, and Figure 10a shows the total phase change computed from both systems.

Finally, Figure 10b shows the result of subtracting the corrected visible phase changeattributed to vibrations, from the total 10.6 μm phase change, leaving the plasma phase change part alone. This has been converted, in the Figure, to electron density integrated along the line of sight.

3.(vi) Phase Comparison Double Interferometer

Double interferometers utilizing an intermediate frequency but replacing quadrature by a phase comparison technique have been used on TFR by Veron (1974), Veron et al (1977), Veron (1979), and on ALCATOR by Wolfe et at (1976). These systems, shown schematically in Figure 11, differ principally in the means adopted to generate the shifted frequency.

Veron utilizes Doppler shift obtained by reflecting a beam in the subsidiary interferometer from a rotating cylindrical blazed grating. The change in frequency is $\Delta\omega = k\ v$, and for reflection at nearly 180° at an angle β to the radius r of the cylinder (Figure 11a)

$$\Delta\omega = \frac{4\ \pi}{\lambda}\ v\ \sin\beta = 8\ \pi^2\ \lambda^{-1} r\ N \sin\beta$$

where N is revolutions per second . With $\beta = 54^\circ$, $\lambda = 337$ μm (HCN laser), $r = 6$ cm , and $N = 5$ rev s^{-1} (Veron et al 1977) this gives shifts of about 10 kHz .

The two detectors produce signals $S_R \sim \cos \Delta\omega\ t$ and $S \sim \cos(\Delta\omega\ t + \varphi)$, and the elapsed time Δt between a positive slope zero crossing of S_R and the nest positive slope zero crossing of S determines the plasma induced phase difference through $\varphi = \Delta t\ \Delta\omega$, as shown in Figure 12 . When the phase difference between S and S_R passes 2π, the elapsed time reaches a maximum equal to the period $2\pi(\Delta\omega)^{-1}$ of the intermediate frequency oscillation, then drops to zero and starts again. If one plots elapsed time as a function of real time during which the excursion of φ exceeds 2π , the display looks like the sketch in Figure 13 . Maximum sensitivity of Veron's instrument is limited by detector noise to about 0.01 fringe .

If plasma conditions are to remain comparatively

static during one period of the intermediate frequency, the latter must satisfy $\Delta\omega >> \frac{2\pi}{n_e}\frac{dn_e}{dt}$. As indicated above, the rotating grating offers typical frequency shifts of about 10 kHz. To procure the substantially larger frequencies near 1 MHz needed to measure much more rapidly changing plasma, Wolfe and his colleagues at MIT used a pair of 1 metre optically pumped 119 μm methyl alcohol lasers. Controlling their cavity length difference to better than 1 μm by a feedback mechanism, this group succeeded in stabilizing their difference frequency to about $\pm$ 2% .

3.(vii) Multiple Beam Interferometry and Data Interpretation

Multiple beam interferometry such as that performed by Veron (1979) on TFR, produces a set of line integrals from which one can recover the two-dimensional distribution whose projections along the probe beams are the data. For an array of parallel beams and a circularly symmetric density distribution, the required inversion is the Abel Transform (Bockasten 1961, Bracewell 1965). Distributions having higher order symmetry or no symmetry at all, such as the quasi-D shapes predicted for JET, call for more advanced methods (Sauthoff and von Goeler 1979).

Williamson and Evans (1982) have discussed this question in terms of conventional matrix inversion. They consider optimizing the location of the probe beams by maximizing their individual freedom from redundancy, and show that an asymmetric arrangement always leads to better reconstruction accuracy than a regular array. They introduce smoothing, and deal with its effect on resolution, channel redundancy, and reconstruction accuracy, and they argue that smoothing should be increased until the natural negative statistical correlations between adjacent picture elements of the two-dimensional source just vanish. They also demonstrate that source function shape can be identified rather sensitively with as few as ten channels provided it conforms to a set which is a member of an already known family.

4. THOMSON SCATTERING

4.(i) Scattering by an Electron Gas: Scattering Form Factor

Laser radiation scattered by the free electrons in the plasma conveys spatially resolved information about electron and ion temperatures, impurities, magnetic field, and microturbulence. Thomson scattering has been the subject of numerous reviews, e.g. Evans and Katzenstein (1969), DeSilva and Goldenbaum (1970), Evans (1974), Segre (1975), Sheffield (1975), Evans (1976), Luhmann (1979), and Magyar (1981). Bernstein (1964) gives a thorough account of the plasma theory involved.

Every charged particle in the plasma scatters radiation, but because the scattering cross-section is inversely proportional to particle mass squared, the contribution from the ions is negligible except in so far as they influence the electrons' motion. Radiation scattering by individual electrons is dipole, and where φ is the angle between the incident radiation electric vector and the direction of the scattered ray, the differential cross-section is

$$\frac{d\sigma}{d\Omega} = r_e^2 \sin^2\varphi \ .$$

Integration over solid angle $d\Omega = 2\pi \sin\varphi \, d\varphi$ results in $\sigma = \frac{8}{3} \pi r_e^2 = 6.65 \times 10^{-25} \text{ cm}^2$.

The electric field radiated to a detector by an electron undergoing acceleration in an incident laser beam is calculated using the Lienard Wiechert potentials of classical electromagnetic theory. Calculation of the field's phase factor using the retarded time and the approximation of rectilinear motion over very short time periods leads to the emergence of the differential scattering vector $\underline{k} = \underline{k}_s - \underline{k}_o$, and the Doppler shifted frequency $\Delta\omega = \underline{k} \cdot \underline{v}$, where $\underline{k}_o$ and $\underline{k}_s$ are the wave vectors of the incident and the scattered radiation, and $\underline{v}$ is the instantaneous electron velocity. The power spectrum of the scattered Poynting flux is found by taking the Fourier transform of the autocorrelation of the field at the detector (Wiener-Khinchine theorem), which results in

$$I = I_o r_e^2 \sin^2\varphi \, n_e \, \ell \, S(\underline{k},\omega) \ . \qquad \ldots(7)$$

Here, I_o is the incident laser power (watts), n_e the electron density, and ℓ the length in plasma over which scattering occurs.

The factor $S(\underline{k},\omega)$ is given by

$$S(\underline{k},\omega) = \frac{1}{2\pi\, n_e\, V} \int_{-\infty}^{+\infty} e^{i(\omega-\omega_o)\tau} < N^*(\underline{k},t)\, N(\underline{k},t+\tau)> d\tau \qquad ...(8)$$

where V is the scattering volume, and $N(\underline{k},t)$ is the Fourier transform of the point density of the electrons in that volume,

$$N(\underline{u},t) = \sum_{j=1}^{N} \delta[\underline{u} - \underline{u}_j(t)] \ .$$

Note that the integral of $S(\underline{k},\omega)$ over the frequency spectrum is

$$S(\underline{k}) = \frac{1}{V} \frac{<|N(k,t)|^2>}{n_e} \ . \qquad ...(9)$$

The simplest case for which $S(\underline{k})$ can be evaluated is that of Raman-Nath scattering, i.e. scattering by a monochromatic density perturbation represented by

$$n(\underline{r}) = n_e + \tilde{n}_e \cos \underline{k}\cdot\underline{r} \ .$$

The Fourier transform of this is

$$n(\underline{k}) = \tilde{n}_e\, V \ , \text{ giving}$$

$$S(\underline{k}) = \frac{1}{V} \frac{\tilde{n}_e^2\, V^2}{n_e} = \frac{\tilde{n}_e^2}{n_e} V \ .$$

Substituting the above into equation (7) and assuming scattering in the dipole equatorial plane ($\sin\varphi = 1$) results in

$$I = I_o\, r_e^2\, \tilde{n}_e^2\, \ell\, V\, \Omega \ ,$$

where Ω, the collection solid angle, has been introduced. The scattering volume V and the solid angle Ω are evaluated from the scattering geometry. Assuming gaussian optics and scattering taking place at a beam waist, half-width W_o, the scattering volume becomes $V = \pi W_o^2\, \ell$, and the solid angle $\Omega = \frac{1}{\pi}(\lambda/2W_o)^2$. The scattering intensity therefore becomes

$$I = \tfrac{1}{4} I_o\, r_e^2\, \lambda^2\, \ell^2\, \tilde{n}_e^2 \qquad ...(10)$$

which is the well known result given by Brillouin's theory for scattering on ultrasonic waves.

4.(ii) Thomson Scattering as a Consequence of Refractivity

It was remarked in the Introduction that Thomson scattering, like interferometry and Faraday rotation, is an effect of refractivity. As a striking demonstration that this is so, it will now be shown, following Evans et al (1982), that the Raman-Nath result derived above from scattering theory, could equally well be obtained from considerations of refraction and diffraction alone.

A basic theorem of Fourier optics (Goodman 1968), stemming from the fact that the propagation of radiation can be completely described in terms of diffraction integrals, is that the amplitude distributions in focal planes on either side of a lens are Fourier transforms of each other, viz

$$U(\xi,\eta) \propto \int_{-\infty}^{+\infty} U(x,y)\, e^{-i\frac{2\pi}{\lambda f}(x\xi + y\eta)}\, dx\, dy \ .$$

Consider a gaussian beam with a beam waist at each focal plane. Let one waist lie in the plasma where a monochromatic wave or phase grating of the form $\Delta\varphi \sin(Kx-\Omega t)$ is travelling perpendicular to the optical axis and so imposes phase shifts on the radiation passing through it. The form of the phase shift depends on the varying refractive index, and is the same as that used in discussing the interferometer, namely $\Delta\varphi = 2\pi \lambda^{-1} L\, \Delta\mu = r_e \lambda L \tilde{n}_e$ for plasma. Thus the gaussian beam having undergone refraction by the phase grating, can be represented by

$$U(x,y)\, e^{i\, \Delta\varphi \sin(Kx-\Omega t)} = \frac{U_o}{\sqrt{\pi}\, W_o} e^{-\frac{x^2+y^2}{2\, W_o^2}} \sum_{\ell=-\infty}^{\infty} J_\ell(\Delta\varphi)\, e^{i\ell(Kx-\Omega t)} \ ,$$

where the phase factor has been expanded into a sum of Bessel functions. The Fourier transform of this expression is performed to obtain $U(\xi,\eta)$ and the latter is multiplied by its complex conjugate to produce an intensity. Finally, under the assumption that phase shift $\Delta\varphi$ is small, the Bessel functions are replaced by their small argument approximations, and the outcome of this whole procedure

is the following expression for the intensity distribution of the beam in the front focal plane of the lens:

$$I(u) = \frac{I_o}{\sqrt{\pi}\, W_f} \Big\{ e^{-u^2} \left[1 - \tfrac{1}{2}(\Delta\varphi)^2\right] + \Delta\varphi\, e^{-\frac{1}{2}v^2} \left[e^{-(u-\frac{1}{2}v)^2} - e^{-(u+\frac{1}{2}v)^2}\right] \cos \Omega t + (\tfrac{1}{2}\Delta\varphi)^2 \left[e^{-(u-v)^2} + e^{-(u+v)^2}\right] + \ldots \Big\} \quad . \qquad \ldots(11)$$

Here, W_f is the beam waist in the front focal plane, $u \equiv \xi/W_f$ is the front focal plane coordinate normalized to W_f, and the dimensionless parameter v relating spot size at the beam waist in the plasma, W_o, to the wave number K of the phase modulation, $v \equiv K W_o$, has been introduced.

The first term above is time-independent and describes the undeviated but slightly attenuated transmitted beam. The small attenuation can be understood as the loss to the main beam of the radiation that appears in the third of the three main terms above. The latter is proportional to $(\frac{1}{2}\Delta\varphi)^2 = \frac{1}{4} r_e^2 \lambda^2 L^2 \tilde{n}_e^2$, and can be recognized as the Thomson scattering of a gaussian beam by a monochromatic electron density wave. The spatial profile of this term, given by the expression in square brackets multiplying it, consists of two gaussian maxima disposed symmetrically on either side of the main beam, and centred at $u = \pm v$ respectively. The equation $u = \pm v$ can readily be shown to be equivalent to the Bragg relation $K = 4\pi \lambda^{-1} \sin \frac{\theta}{2}$ for small scattering angle θ. We emphasize again that this term has appeared spontaneously in a treatment based exclusively on refraction and diffraction.

4.(iii) Form Factor for a Field Free, Cool, Thermal Plasma

A general expression for the form factor $S(\underline{k},\omega)$ for a magnetic field free thermal plasma was calculated using the Nyquist dissipation theorem by Dougherty and Farley (1960), and using methods of plasma kinetic theory, by Akhiezer et al(1957), Salpeter (1960), Fejer(9160), and Hagfors (1961). They showed that in terms of the dielectric susceptibilities

of the electrons and the ions, G_e and G_i, respectively, the form factor can be written

$$S(k,\omega) = \frac{|1-G_i|^2 F_e + Z|G_e|^2 F_i}{|1 - G_e - G_i|^2} \qquad \ldots(12)$$

where F_e and F_i are the Maxwellian velocity distributions of the electrons and the ions. Moreover G_e and G_i are both proportional to the Fried and Conte (1961) plasma dispersion function (Figure 14)

$$W(x) = 1 - 2x\, e^{-x^2} \int_0^x e^{t^2} dt - i\sqrt{\pi}\, x\, e^{-x^2}$$

with $G_e = -\alpha^2 W$ and $G_i = -Z\,(T_e/T_i)\,\alpha^2 W$.
Here Ze is the ion charge, T_e and T_i the electron and ion temperatures, and $\alpha \equiv (k\lambda_D)^{-1}$ is the ratio of the scattering scale length k^{-1} to the plasma Debye length λ_D. The variable $x \equiv \omega/k\,v$, v being the thermal velocity.

The form factor frequency distribution has the general character illustrated in Figure 15, the wide low intensity part coming mainly from the first term in equation (12) and the narrow high intensity central maximum coming from the second term. These have been called the electron and ion terms respectively. When the parameter $\alpha \ll 1$ the ion term is virtually absent and $S(k,\omega) \approx F_e$. When $\alpha \gtrsim 1$ the susceptibilities no longer vanish and the ion term dominates the spectrum.

$$\text{Provided } \beta^2 \equiv \frac{\alpha^2}{1+\alpha^2} Z(T_e/T_i) < \frac{-1}{\mathrm{Re}[W(x)]_{min}} \approx 3.5$$

the form factor can be approximated by

$$S(k,\omega) = a_e \Gamma_\alpha(a_e x) + Z\left(\frac{\alpha^2}{1+\alpha^2}\right)^2 \Gamma_\beta(x)$$

which is the approximation due to Salpeter (1960).
Here $a_e^2 \equiv (m_e/M)(T_i/T_e)$ and $\Gamma_{\alpha,\beta}(u) \equiv |1+(\alpha,\beta)^2 W(u)|^{-2}\, e^{-u^2}$ with $x \equiv \omega/kv_i$. Figure 16 shows how the spectral distribution of the ion term varies with the parameter β. With β small it is almost gaussian with width kv_i being

a measure of ion temperature T_i. If β lies in the range $1 < \beta < \sqrt{3.5}$ the ion feature has maxima at the ion plasma frequency $\pm \omega_{pi}$ for $\alpha \sim 1$, and goes over into ion acoustic waves at frequency $k\,[KT_e Z/M]^{\frac{1}{2}}$ as α increases.

For more than a decade, experiments using giant pulse ruby lasers have confirmed the details of the thermal theory, in particular with respect to the collective ion feature. Most are summarized in Sheffield (1975). Recent advances have entailed the use of pulsed CO_2 lasers e.g. Pasternak and Offenberger (1977) and Peebles and Herbst (1978). Massig (1978) even succeeded in measuring the thermal ion spectrum of a hydrogen arc using a 20 watt CW CO_2 system.

Representative single discharge ion features measured in the Culham plasma focus with a pulsed ruby and a gated optical multichannel analyser (OMA) are shown in Figure 17 (Kirk 1982).

4.(iv) Impurities

The theory is readily extended to describe plasmas containing more than a single ion species, i.e. impurities, and the form factor for scattering then becomes (Evans 1970)

$$S(k,\omega) = \frac{\left|1 - \Sigma G_j\right|^2 F_e + \left|G_e\right|^2 \frac{1}{n_e} \Sigma Z_j^2 N_j F_j}{\left|1 - G_e - \Sigma G_j\right|^2} \qquad \ldots(13)$$

where now G_j is the susceptibility for ions of type j. N_j is the number of j-type ions, and F_j is their velocity distribution. Modest impurity levels can produce striking changes in the frequency spectrum, for example that of a hydrogen plasma contaminated by 5% fully stripped oxygen will be dominated by the oxygen. Stamatakis (1981) has used the above expression to calculate spectra for a hydrogen-deuterium plasma is which the relative abundance of the two components varies from pure hydrogen to pure deuterium. The result is shown in Figure 18. Because the effective charge $\overline{Z} \equiv \Sigma Z_j^2 N_j / n_e$ appears explicitly, collective scattering may offer an attractive alternative to spectroscopy as a means of making a localized measurement

of this important quantity (Evans and Yeoman 1974, Bretz 1976).

Kasparek et al (1980) and Kasparek and Holzhauer (1981) have measured ion features in a hydrogen arc with admixtures of helium, nitrogen, and argon. Their results (Figure 19) are the first unambiguous experimental confirmation of the theoretical model just outlined for a multi-constituent plasma.

4.(v) Ion Temperature in Fusion Research Tokamaks

Determination of ion temperatures near the centre of fusion research plasmas using the conventional charge exchange neutrals technique will meet difficulties in the new generation of large tokamaks whose dimensions (typically $\gtrsim$ 1 metre minor diameter) will inhibit the escape of neutrals from the central regions. Collective Thomson scattering offers an attractive alternative, and pilot experiments at 10.6 μm on PDX (Taylor and Bretz 1981) and at 385 μm on ALCATOR C (Woskoboinikow et al 1981) are currently being conducted. Detection in both cases exploits the advantages of heterodyne receivers, including discrimination against stray radiation at small scattering angle, and the capacity to extract weak signal from noise.

The theory of heterodyne detection (Cummins and Swinney 1970) shows that when a weak optical field having its intensity distributed over frequency according to some function $I_s(\nu)$ and a strong local oscillator at a fixed unique frequency $\nu_{\ell o}$ are superimposed on a square law detector under conditions that meet the requirements of the van Cittert and Zernike coherence theorem (Born and Wolf, 1964), the resulting detector current i has a power spectrum $P_i(\nu)$ proportional to $i_{\ell o}$, the detector current due to the local oscillator alone, and to $I_s(\nu-\nu_{\ell o})$, the intensity spectrum of the weak radiation transposed to the beat frequency $\nu-\nu_{\ell o}$.

That this is plausible can be seen by taking the beat frequency component of the detector current to be proportional to the square of the sum of the electric fields associated with the signal and with the local oscillator, i.e.

$$i \sim \left| E_s + E_{\ell o} \right|^2 = I_s + I_{\ell o} + 2\sqrt{(I_s\, I_{\ell o})} \cos 2\pi(\nu-\nu_{\ell o})t \ .$$

The frequency analysing network in turn generates an output which is proportional to the square of the beat frequency term:

$$i_{out} \sim i^2 \sim I_{\ell o} I_s \sim i_{\ell o} I_s .$$

The power spectrum is given by (Cummins and Swinney 1970, equation 2.19)

$$P_i(\nu) = e\, i_{\ell o} + 2\pi\, i_{\ell o}^2\, \delta(\nu) + i_{\ell o} \langle i_s \rangle \int_{-\infty}^{\infty} [e^{2\pi i(\nu+\nu_{\ell o})\tau}\, g_s^1(\tau) + e^{2\pi i(\nu-\nu_{\ell o})\tau}\, g_s^1(\tau)^*]\, d\tau \quad \ldots(14)$$

In this expression $g_s^1(\tau)$ is the normalized first order autocorrelation function of the weak radiation field, defined by

$$g_s^1(\tau) \equiv \frac{\langle E_s^*(t) E_s(t+\tau) \rangle}{\langle E_s(t)^2 \rangle} = \frac{e\,\eta}{h\,\nu}\, \varepsilon_o c\, \frac{\langle E_s^*(t) E_s(t+\tau) \rangle}{\langle i_s \rangle}$$

since $\langle i(t) \rangle = \frac{e\eta}{h\nu} \langle I(t) \rangle = \frac{e\eta}{h\nu}\, \varepsilon_o c\, \langle E(t)^2 \rangle$.

Here, i_s is the detector current due to the weak field alone, $E_s(t)$ is its time-dependent electric field, η is the detector quantum efficiency, and the other symbols have their usual meanings. Substituting $g_s^1(\tau)$ into the integral term of $P_i(\nu)$ and dropping the first part of the integrand which is at the sum rather than the difference frequency and is generally physically unobserable for that reason, yields

$$i_{\ell o} \frac{e\eta}{h\nu}\, \varepsilon_o c \int_{-\infty}^{\infty} e^{2\pi i(\nu-\nu_{\ell o})\tau} \langle E_s^*(t) E_s(t+\tau) \rangle^*\, d\tau$$

which $= i_{\ell o} \frac{e\eta}{h\nu}\, I_s(\nu-\nu_{\ell o})$ by the Wiener-Khinchine theorem.

The first term in equation (14) represents shot noise, the second, of which a factor is the Dirac delta function, is absent except at zero frequency, and the third is the heterodyne spectrum. The latter can now be seen to be an exact replica of the optical spectrum, but centred at a frequency equal to the difference between the weak field

and the local oscillator frequencies. It is this power spectrum that one seeks to measure.

Using equation (14), the signal-to-noise ratio s in the detector photocurrent can be written

$$s = \frac{\text{signal}}{\text{noise}} = \frac{i_{\ell_o}(e\eta/h\nu)\ I_s(\nu-\nu_{\ell_o})}{e\ i_{\ell_o} + \text{electronics noise}} \quad .$$

The foregoing expression shows that if the local oscillator is so strong that the first term in the denominator $e\ i_{\ell_o}$, the shot noise, dominates other noise contributions, then s becomes independent of the local oscillator current i_{ℓ_o} and is given simply by

$$s = \frac{I_s(\nu-\nu_{\ell_o})}{h\nu/\eta} \quad .$$

In these circumstances, the detector noise equivalent power (N.E.P.), that is, the value the signal must take to make $s = 1$, is precisely $h\nu/\eta$.

The detector current i is either processed by an electronic spectrum analyser (for details, see Sharp et al 1980, Appendix) or digitized and processed numerically (Green et al 1980). In either case an output proportional to $P_i(\nu)$, the detector current power spectrum, is generated. It is this output current that is actually measured, and it has both signal and noise components. The signal-to-noise ratio S in this output current is related to that of the detector current, s, through

$$S = \frac{s}{1+s}\sqrt{(1 + \Delta\nu\ T)}$$

where $\Delta\nu$ is the bandwidth of the detector channel resolution interval and T is the integration time, or pulse length in the case of a pulsed laser experiment. Clearly output signal-to-noise S depends strongly on s only if the latter is less than one. If $s \gg 1$, $S \sim \sqrt{(1+\Delta\nu\ T)}$ and is consequently independent of input signal-to-noise. It is then determined exclusively by the parameters of the frequency analysing circuit and the pulse length, and no significant improvement can be effected by increasing the input signal-to-noise.

The value of S required to enable ion temperature to be determined to any desired accuracy has been investigated by the Lausanne group (Green et al 1980) and by Sharp et al(1981) . In both studies, Monte Carlo techniques were used to generate numerical simulations of noisy spectra, and the best fits between simulated and theoretical distributions were identified by chi-square testing. It was concluded that ion temperatures could be measured to an accuracy of a few 10's of per cent if $S \gtrsim 2$, and if $S = 10$, the accuracy of T_i could approach 10% . Estimates of impurity contamination were very much less accurate, but the presence of up to 2% fully stripped oxygen had no adverse influence on the temperature estimate. Perhaps the most important conclusion was that the required values of S could be achieved in the new hot tokamak plasmas only if laser pulses could be sustained for up to a few microseconds.

4.(vi) Hot Plasma Electron Temperature: Relativistic Treatment

Incoherent scattered radiation for which the form factor is simply the electrons' one dimensional Maxwell velocity distribution has served for many years as a routine and reliable means for measuring plasma electron temperature. While temperatures remained below a few hundred electron volts only imperceptible errors resulted from ignoring relativistic effects. But even by 1978 the PLT plasma temperature had reached 5 keV (Eubank et al 1978), and much higher temperatures are anticipated in the new generation of fusion research assemblies now under construction or being contemplated. Revision of elementary theory to take relativity into account has been necessary to predict correctly the scattered radiation frequency distributions expected in these plasmas.

The relativistic expression for the frequency spectrum of radiation incoherently scattered by a hot plasma is found by integrating the contribution from a single electron over the relativistic Maxwell velocity distribution. For a single electron, the scattered electric field at a detector remote

from the plasma can be shown to be

$$\underline{E} = r_e \frac{\sqrt{(1-\beta^2)}}{(1-\beta_s)^3 u} \underline{E}_i \left[\beta_E^2(1-\cos\theta)-(1-\beta_i)(1-\beta_s)\right]$$

where the electron velocity $\underline{v} \equiv \underline{\beta}c$, and β_i, β_s , and β_E are components of $\underline{\beta}$ in the directions of the incident beam, the scattered beam, and the incident beam electric field vector respectively. The symbol θ represents the scattering angle between the incident and scattered beam directions, and incident and scattered beams are polarized perpendicular to the scattering plane. The u in the denominator is the distance from the electron to the detector.

We define the scattering cross-section per unit solid angle $\frac{d\sigma}{d\Omega}$ as the rate at which energy reaches the detector during a finite period of electron acceleration, divided by the incident Poynting flux $\epsilon_o c E_i^2$. Following standard treatments, e.g. Jackson (1962) p.472, Panofsky and Phillips (1955) p.302 , Landau and Lifshitz (1975) p.194 , we note that the energy reaching a detector from an electron undergoing acceleration from retarded time T_1 to T_2 is

$$\int_{t=T_1+\frac{u(T_1)}{c}}^{T_2+\frac{u(T_2)}{c}} \epsilon_o c E^2 u^2 d\Omega \, dt = \int_{t'=T_1}^{T_2} \epsilon_o c E^2 u^2 d\Omega \frac{dt}{dt'} \, dt'$$

where $t'=t-\frac{u(t')}{c}$ is the retarded time, and $\frac{dt}{dt'} = 1-\beta_s$. Accordingly

$$\frac{d\sigma}{d\Omega} = r_e^2 \frac{1-\beta^2}{(1-\beta_s)^5} \left[\beta_E^2(1-\cos\theta) - (1-\beta_i)(1-\beta_s)\right]^2 . \qquad \ldots(15)$$

The foregoing expression differs from what one would calculate using simply the Poynting flux associated with the field $\underline{E}$ at the detector, by an extra factor $(1-\beta_s)$ in the numerator. Pechacek and Trivelpiece (1967) drew attention to the need to include this factor and subsequently offered experimental evidence in support of their argument (Ward et al, 1971; Ward and Pechacek, 1972).

The relativistic Maxwell distribution, normalized

to unity, is (Watson et al 1960)

$$f(\beta) = [2\pi K_2(2c^2/v_e^2)]^{-1} \frac{c^2}{v_e^2} (1-\beta^2)^{-5/2} e^{-2\frac{c^2}{v_e^2}(1-\beta^2)^{-1}}$$

where $v_e \equiv (2KT_e/m)^{\frac{1}{2}}$, and $K_2(\ )$ is a modified Bessel function of the second kind, of order 2 (tabulated in, for example, Abramowitz and Stegun 1965) . It is easy to verify that the Doppler shift experienced by the radiation can be expressed as

$$\frac{\omega_s}{\omega_i} = \frac{1-\beta_i}{1-\beta_s}$$

where ω_s and ω_i are frequencies of the scattered and incident radiation respectively, so the scattered radiation frequency spectrum should be

$$r_e^2 S(\omega_s) = \iiint \frac{d\sigma}{d\Omega} f(\beta) \delta\left(\frac{\omega_s}{\omega_i} - \frac{1-\beta_i}{1-\beta_s} \right) d^3\underline{\beta} \quad .$$

A first order approximation to this integral was obtained by Sheffield (1972), and Matoba et al (1979) have published a second order formula. By taking a mean value for the polarization term

$$q = \left[1 - \frac{(1-\cos\theta)}{(1-\beta_i)(1-\beta_s)} \beta_E^2\right]^2 \leq 1 \quad \text{(see equation 15 above)}$$

Zhuralev and Petrov (1979) have succeeded in expressing the integral in closed analytic form, and Selden (1980) has reduced this to a result suitable for routine experimental analysis, viz

$$S(\epsilon,\theta) = q\,[2K_2(2c^2/v_e^2)\, A(\epsilon,\theta)]^{-1}\, e^{-(2c^2/v_e^2)\, B(\epsilon,\theta)}$$

where $\epsilon \equiv \frac{\omega_i}{\omega_s} - 1$

$$A(\epsilon,\theta) \equiv (1+\epsilon)^2 [2(1+\epsilon)(1-\cos\theta) + \epsilon^2]^{\frac{1}{2}}$$

$$B(\epsilon,\theta) \equiv \left[1 + \epsilon^2 \left\{ 2(1+\epsilon)(1-\cos\theta) \right\}^{-1}\right]^{\frac{1}{2}} \quad .$$

Figure 20 shows frequency distributions calculated with

this expression for plasmas with temperatures up to 50 keV . They display the characteristic blue shift of the maximum associated with the forward bias in the radiation pattern of the relativistic electrons.

Hot plasma incoherent scattering has received so much attention because of its practical importance for measuring electron temperature. By contrast, the role of relativity in collective scattering has suffered neglect on the grounds, presumably, that the small frequency shifts involved correspond to subrelativistic phase velocities, ignoring the fact that the electrons actually doing the scattering may be very relativistic indeed. This is an area that would repay attention at the present time.

Acknowledgements

My thanks are due to all my colleagues who assisted in the preparation of this article. I am particularly indebted to David Muir who advised me on Faraday rotation, and to Adrian Selden who gave me the benefit of his understanding of the role of relativity in plasma scattering.

References

Abramowitz M. and Stegun I.A. (1965)
Handbook of Mathematical Functions
pub Dover Publications Inc.

Akhiezer A.I., Prokgoda I.G., and Sitenko A.G. (1957)
Zh. Eksp. Teor. Fiz. (USSR) 33 750-

Alpher R.A. and White D.R. (1965) Optical Interferometry,
Chap 10 in Plasma Diagnostic Techniques
ed. Huddleston R.H. and Leonard S.L.
pub. Academic Press Inc.

Ashby D.E.T.F. and Jephcott D.F. (1963)
Applied Physics Letters 3 13-

Baker D.R. and Shu-Tso Lee (1978)
Rev Sci Instrum 49 919-922

Berger J. and Lovberg R.H. (1970) Science 170 296-

Bernstein I.B., Trehan S.K., and Weenink M.P. (1964)
Nuclear Fusion 4 61-

Birch J.R. and Jones R.G. (1970) Infrared Physics 10 217-

Bockasten K. (1961) J. Opt. Soc. Amer. 51 943-

Born M. and Wolf E. (1964) Principles of Optics
pub. Pergamon Press

Bracewell R. (1965) The Fourier Transform and Its
Applications p 262 et seq pub. McGraw-Hill

Bretz N.L. (1977) Applied Physics Letters 31 372-374

Brown R., Deuchars W.M., Illingworth R., and Irving J.
(1977) J.Phys. D 10 1575-1581

Buchenauer C.J. and Jacobson A.R. (1977)
Rev Sci Instrum 48 769-774

Craig A.D. (1976) Plasma Physics 18 777-790

Cummins H.Z. and Swinney H.L. (1970) Progress in Optics
Vol 8 p.135 et seq pub North Holland

DeMarco F. and Segre S.E. (1972) Plasma Physics 14 245-252

DeSilva A.W. and Goldenbaum G. (1970) Chap 3 in
Methods of Experimental Physics Vol 9 Pt A
ed. Lovberg R.H. and Griem H.R.
pub. Academic Press Inc.

Dodel G. and Kunz W. (1978) Infrared Physics 18 773-776

Dougal A.A., Craig J.P. and Gribble R.F. (1964)
Phys Rev Letters 13 156-158

Dougherty J.P. and Farley D.T. (1960)
Proc Roy Soc A 259 79-

Evans D.E. (1970) Plasma Physics 12 573-584

Evans D.E. (1974) Optical Methods of Plasma Diagnostics
Chap 6 in Plasma Physics ed. Keen B.E.
pub. in Conference Ser. No. 20 by The Institute
of Physics, London

Evans D.E. (1976) Physica 82C 27-42

Evans D.E., von Hellermann, M. and Holzhauer E. (1982)
Plasma Physics

Evans D.E. and Katzenstein J. (1969)
Reports of Progress in Physics 32 207-271

Evans D.E. and Yeoman M.L. (1974)
Phys Rev Letters 33 76-78

Eubank H., Goldston R. Arunasalam V. (1978)
7th International Conference on Plasma Physics
and Controlled Nuclear Fusion Research, Innsbruck
CN-37 C3

Falconer I. and Ramsden S.A. (1968)
J. Appl. Physics 39 3449-3458

Fejer J.A. (1960) Can. J. Phys. 38 1114-

Frayne P.G. (1968) J Phys D 1 741-

Fried B.D. and Conte S.D. (1961)
The Plasma Dispersion Function pub. Academic Press Inc.

Gibson A. and Reid G.W. (1964)
Appl Phys Letters 5 195-197

Goodman J.W. (1968) Introduction to Fourier Optics
pub. McGraw-Hill

Gowers C.W. and Lamb C. (1982) J Phys E

Green M.R., Morgan P.D., Siegrist M.R. and Watterson R.L. (1980)
CRPP Ecole Polytechnique Federale de Lausanne-Suisse
Report LRP 168/80

Hagfors T. (1961) J Geophys Research 66 1699-

Heald M.A. and Wharton C.B. (1965)
Plasma Diagnostics with Microwaves
pub John Wiley and Sons Inc.

Heller W. (1960) in Physical Methods of Organic Chemistry
ed. Weissberger Vol I Pt.3 2180-2332
pub. Interscience Pub. Inc.

Heym A. (1968) Plasma Physics 9 1069-

Hugenholtz C.A.J. and Meddens B.J.H. (1979)
Rev Sci Instrum 50 1123-1124

Jackson J.D. (1962) Classical Electrodynamics Chap 14
pub John Wiley and Sons Inc

Jacobson A.R. and Call D.L. (1978)
Rev Sci Instrum 49 318-320

Jahoda F.C. and Sawyer G.A. (1971) Optical Refractivity
of Plasmas in Methods of Experimental Physics
Vol 9 : Plasma Physics Pt B ed. Lovberg R.H. an Griem H.R.
pub Academic Press Inc

Kasparek W., Hirsch K., and Holzhauer E. (1980)
Plasma Physics 22 555-558

Kasparek W. and Holzhauer E. (1981) Univ of Stuttgart
Institute for Plasma Science Report IPF-81-5

Kirk R.E. (1982) Ph D thesis University of London
(Royal Holloway College)

Kunz W. and Dodel G. (1978) Plasma Physics 20 171-174

Kunz W. and Equipe TFR (1978) Nuclear Fusion 18 1729-1732

Landau L.D. and Lifshitz E.M. (1975) The Classical Theory
of Fields (trans Morton Hamermesh) pub. Pergamon Press

Luhmann Jr.,N.C. Instrumentation and Techniques for Plasma
Diagnostics Chap I in Infrared and Millimeter Waves
Vol 2 : Instrumentation
ed Button K.J. pub Academic Press Inc (1979)

Magyar G. (1981) Plasma Diagnostics Using Lasers
Chap 23 in Plasma Physics and Nuclear Fusion Research
ed Gill R.D. pub Academic Press Inc

Massig J.H. (1978) Physics Letters 66A 207-209

Massig J.H. (1978) Institut fur Plasmaforschung der
Universitat Stuttgart, preprint IPF 78-2

Matoba, Tohru Itagaki T., Yamauchi T., and Funahashi A.(1979)
Jap Journ of Appl Physics 18 1127-1133

Panofsky W K H and Phillips M (1955) Classical Electricity and Magnetism Addison Wesley Publishing Company

Pasternak A W and Offenberger A A (1977) Can J Phys 55 419-427

Pechacek R E and Trivelpiece A W (1967) Physics of Fluids 10 1688-1696

Peebles W A and Herbst M J (1978) IEEE Transactions on Plasma Science PS-6 564-567

Ramachandran G N and Ramaseshan S (1961) Crystal Optics Encyclopedia of Physics Vol 25/1 pub Springer

Salpeter E E (1960) Physical Review 120 1528-1535

Segre S E (1975) Course on Plasma Diagnostics and Data Acquisition 265-301 ed. Eubank H and Sindoni E pub Editrice Compositori, Bologna

Segre S E (1978) Plasma Physics 20 295-307

Selden A C (1980) Physics Letters 79A 405-406

Selden A C (1982) Culham Report CLM R220

Siegman A E (1971) An Introduction to Lasers and Masers pub McGraw-Hill

Sharp L E, Sanderson A D, and Evans D E (1980) Culham preprint CLM P548

Sharp L E, Sanderson A D, and Evans D E (1981) Plasma Physics 23 357-370

Sheffield J (1972) Plasma Physics 14 783-

Sheffield J (1975) Plasma Scattering of Electromagnetic Radiation pub Academic Press Inc

Stamatakis T (1981) private communication (Appendix to JET report)

Taylor G and Bretz N L (1981) Bull Amer Phys Soc 26 991

Veron D (1974) Optical Communications 10 95-

Veron D (1979) Submillimetre Interferometry of High Density Plasmas, Chap 2 in Infrared and Submillimeter Waves Vol 2 : Instrumentation ed K J Button pub Academic Press Inc

Veron D, Certain J, and Crenn J P (1977) J Opt Soc Amer 67 964-967

Ward G and Pechacek R E (1972) Phys of Fl 15 2202-2210

Ward G, Pechacek R E, and Trivelpiece A W (1971) Physical Review A3 1721-1723

Watson K M, Bludman S A and Rosenbluth M N (1960)
Physics of Fluids 3 741-

Williamson J H, and Evans D E (1982)
IEEE Transactions on Plasma Science

Wolfe S M, Button K J, Waldman J, and Cohn D R (1976)
Applied Optics 15 2645-2648

Wood R W Physical Optics pub Dover Publications Inc (1967)

Woskoboinikow P, Mulligan W J , Cohn D R, Fetterman H,
Praddaude H C, and Lax B (Sept 1981)
Bull Amer Phys Soc 26 922

Zhuralev V A , and Petrov G.D. (1979)
Soviet Journal of Plasma Physics 5 3-5

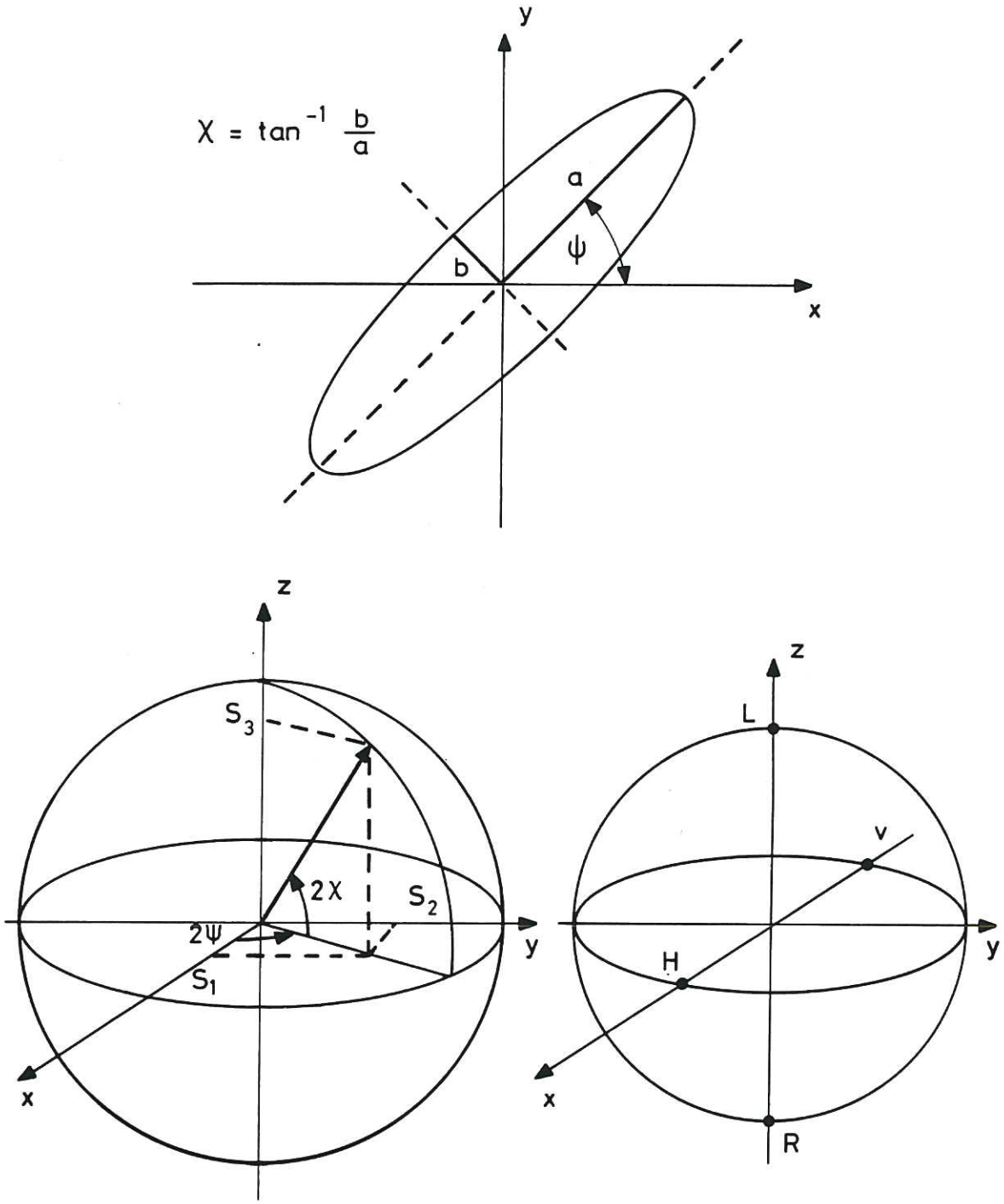

Fig.1 Vibrational ellipse for electric vector of polarised wave, specifying ψ and χ, from which the Stokes parameters S_1, S_2 and S_3 are calculated, defining a point on the Poincaré sphere. H = horizontal, V = vertical L and R = left and right hand circularly polarised.

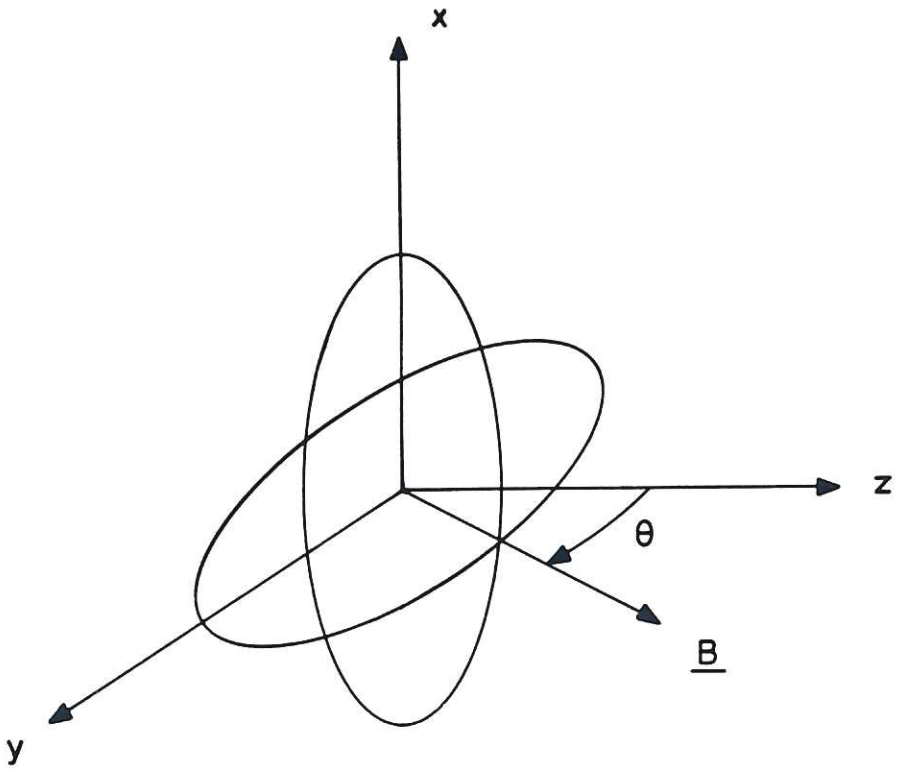

Fig.2 Characteristic waves in magnetised plasma. Radiation propagates in +z direction. Magnetic field $\underline{B}$ lies in y–z plane at angle θ to +z axis.

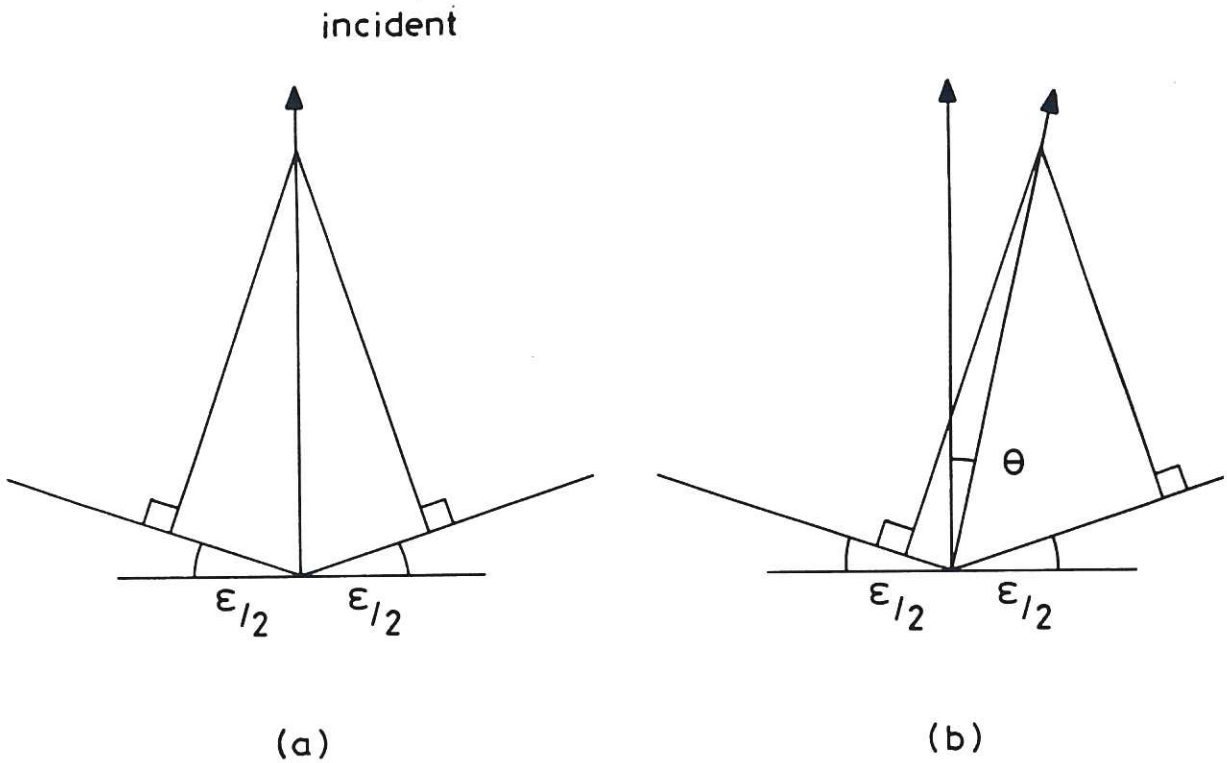

Fig.3 Half shade method for Faraday rotation measurement. Analysers are set ½ϵ radians away from perpendicular to incident beam polarisation.

(a) no rotation

(b) rotation through small angle θ.

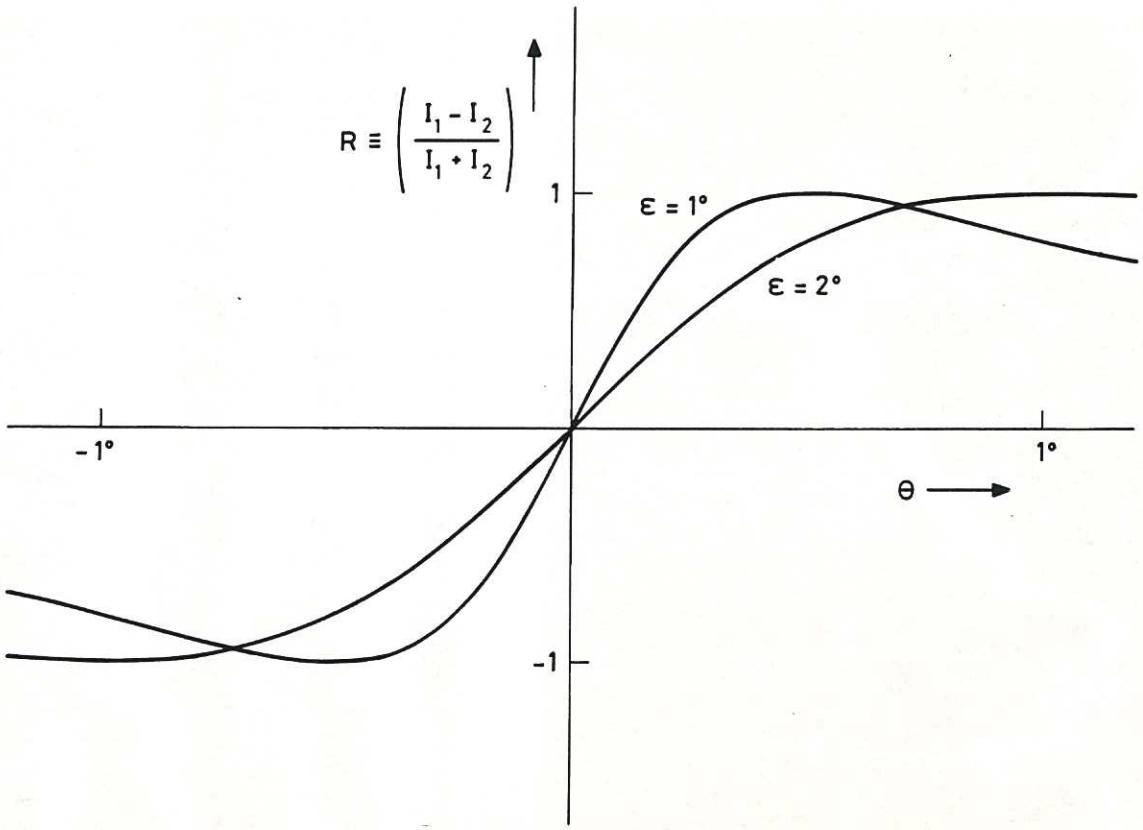

Fig.4 Analysis of half shade angle method. I_1 and I_2 are intensities transmitted through the two analysers, set at angle ½ε. Angle θ is rotation undergone by probe beam polarisation.

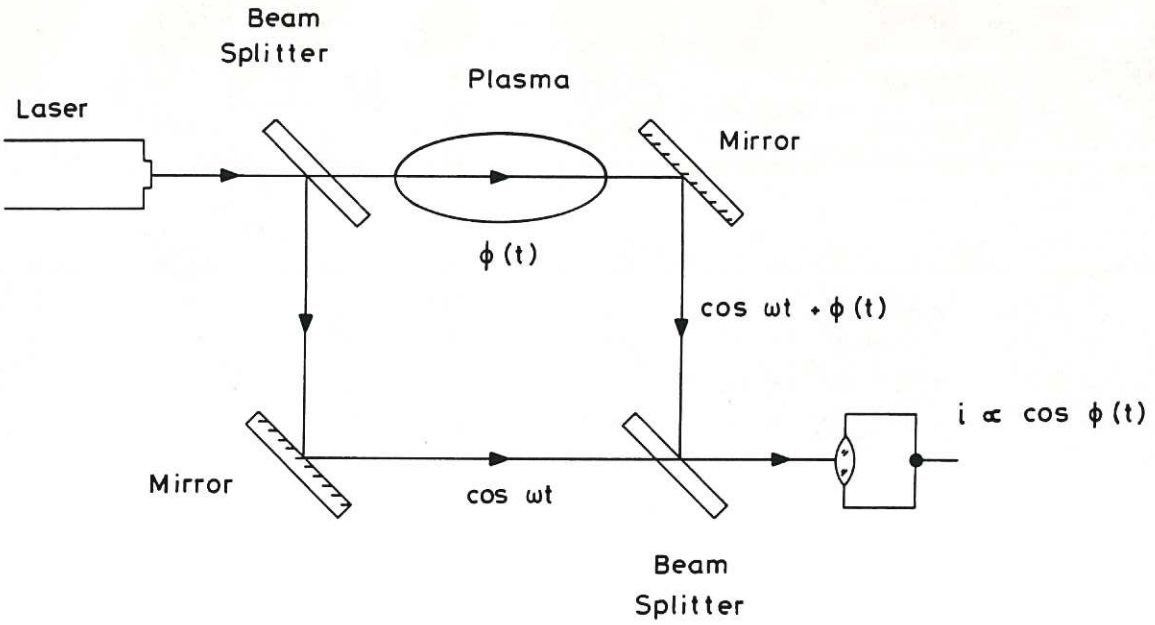

Fig.5 Primitive Mach-Zehnder interferometer. Probe beats with reference on square law detector to produce current proportional to cosine of phase difference introduced in probe by plasma.

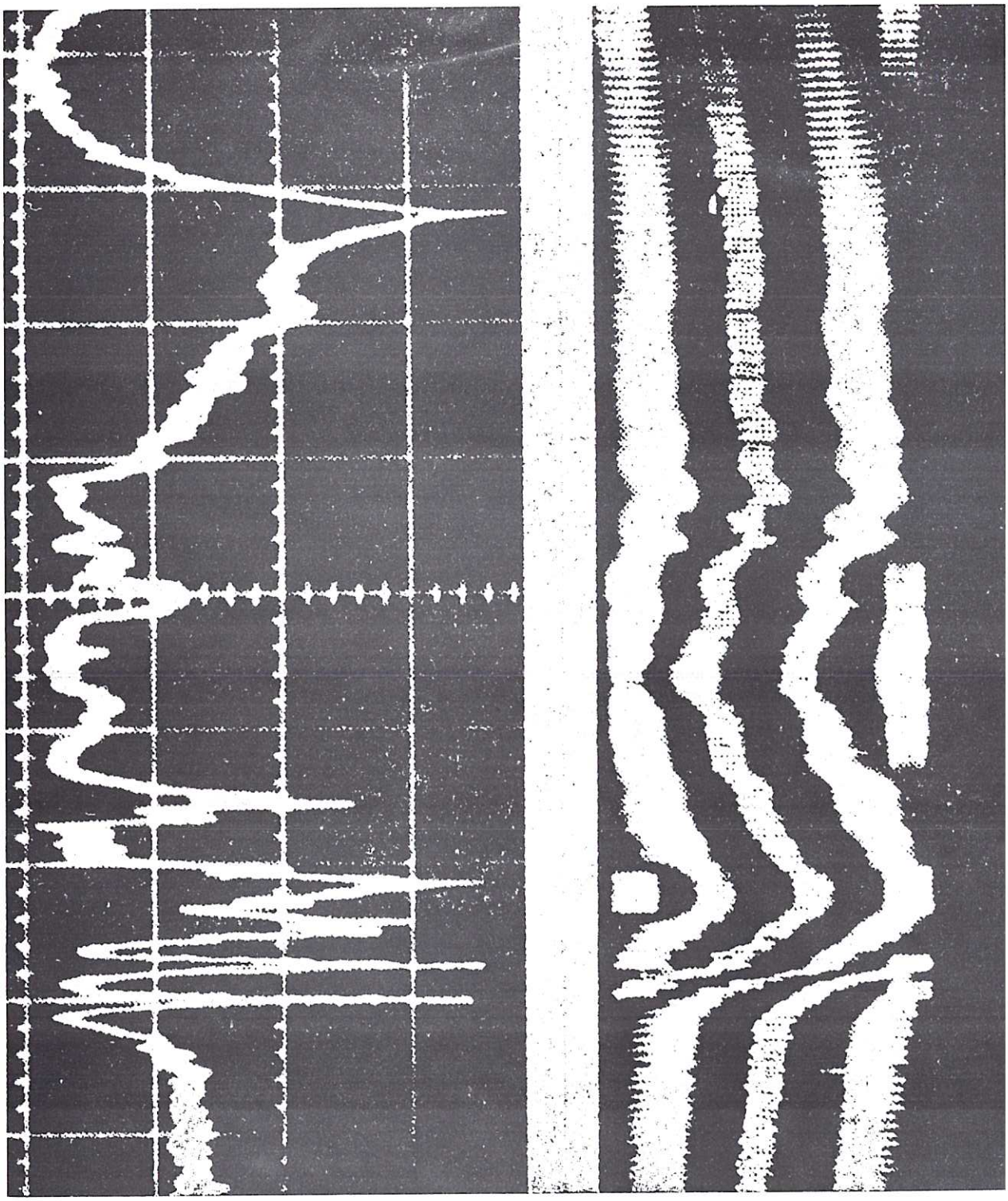

Fig.6 Raw interferometer output and zebra-stripe display of a similar plasma discharge, from Gibson and Reid (1964)

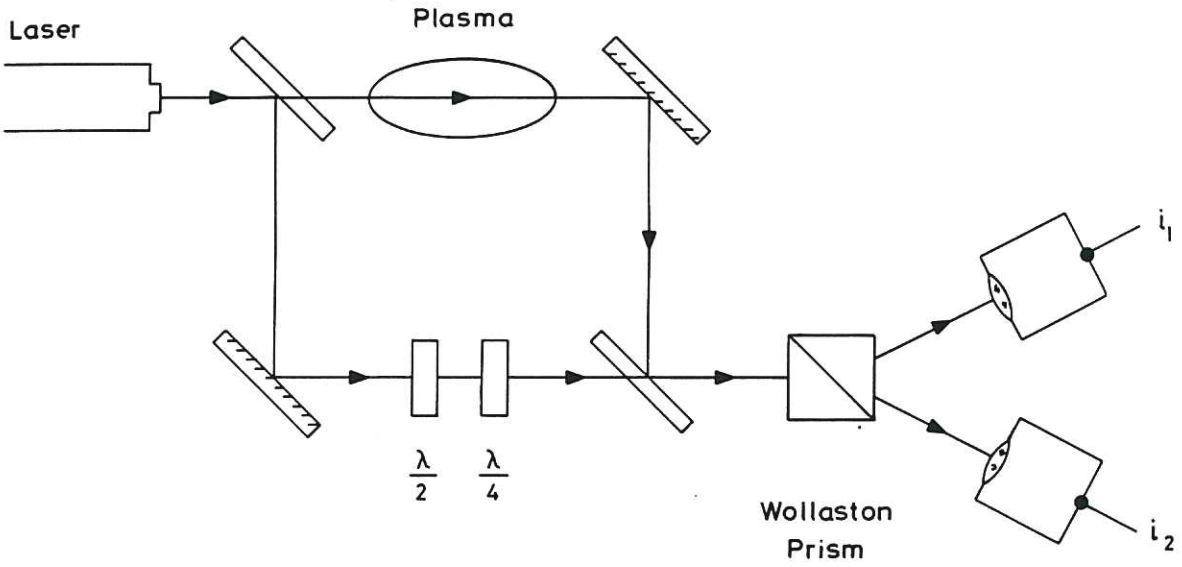

Fig.7a Phase quadrature arrangement, after Buchenauer and Jacobson (1977). Retardation plate (¼λ) circularly polarises reference beam as it enters the Wollaston prism. Probe remains plane polarised. The ½λ plate compensates residual ellipticity of reference beam induced by beam splitter and mirror.

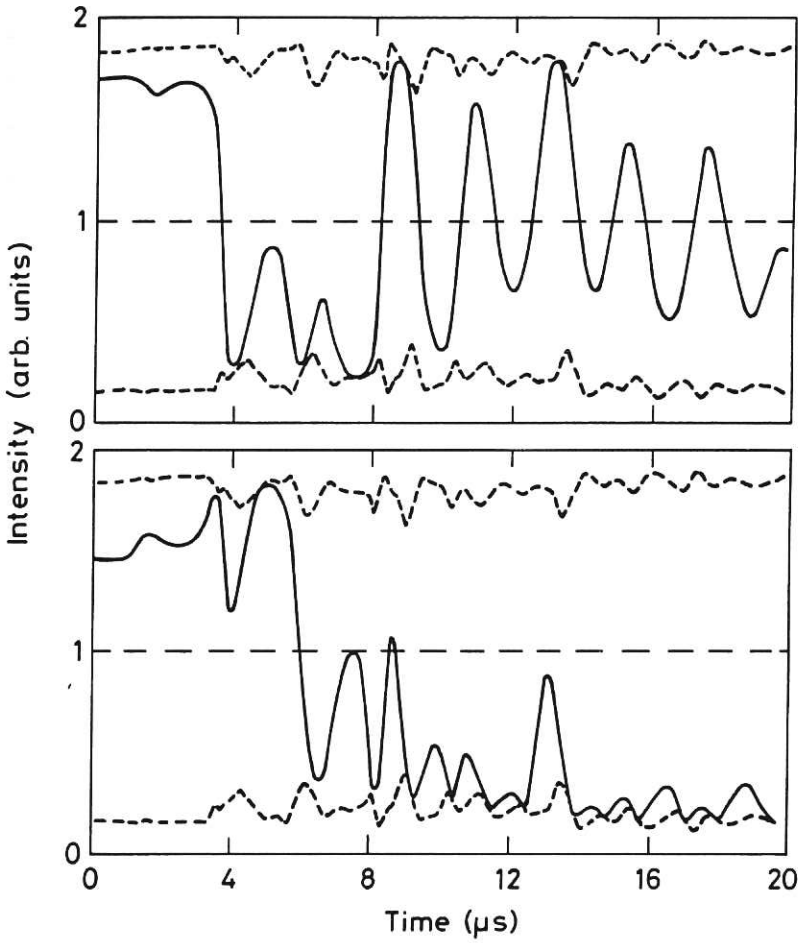

Fig.7b Signals in quadrature produced by the pair of detectors above. Short dashes are calculated fringe envelope extrema. After Buchenauer and Jacobson (1977).

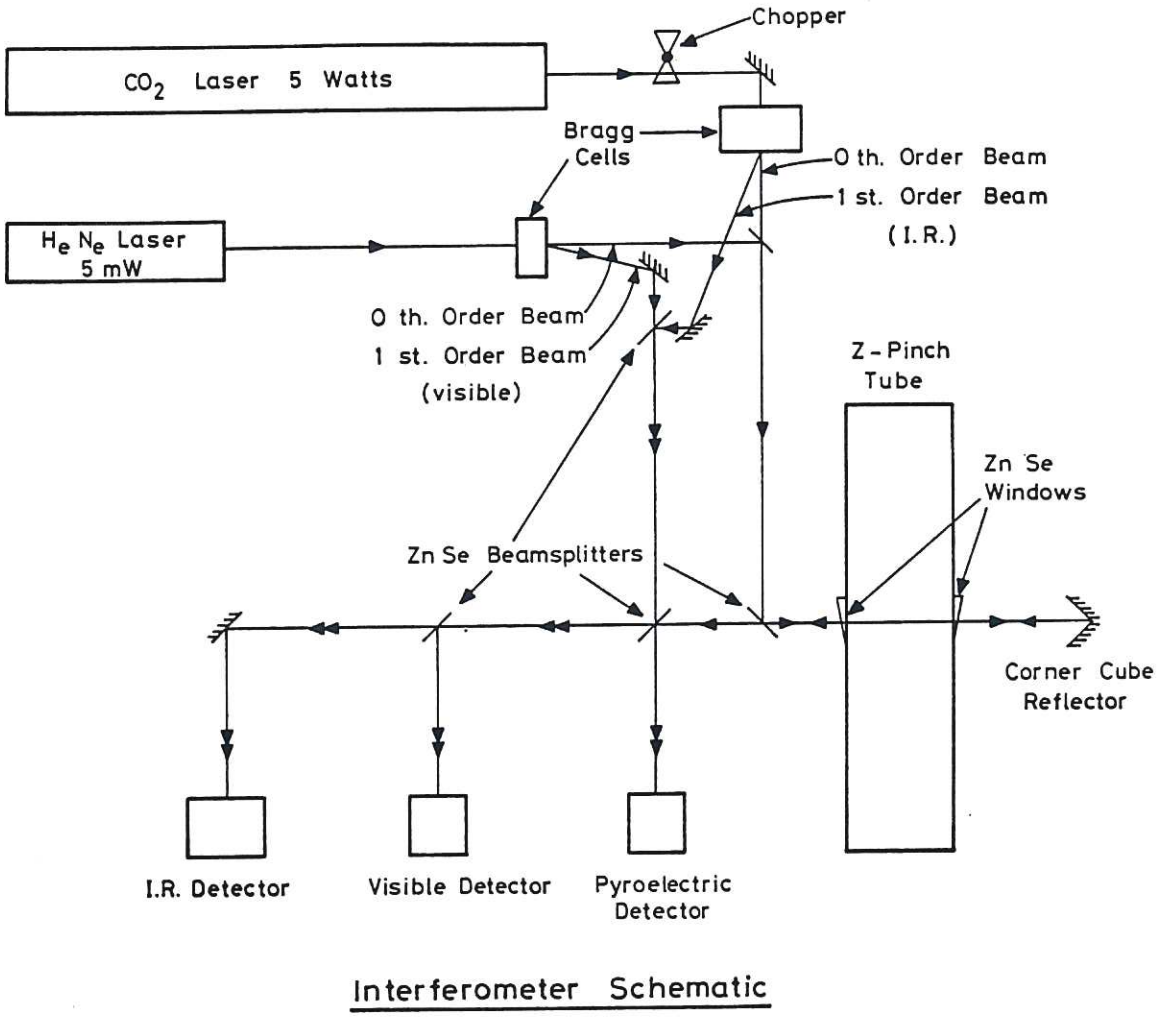

Fig.8 Vibration compensated quadrature interferometer of Gowers and Lamb (1982).

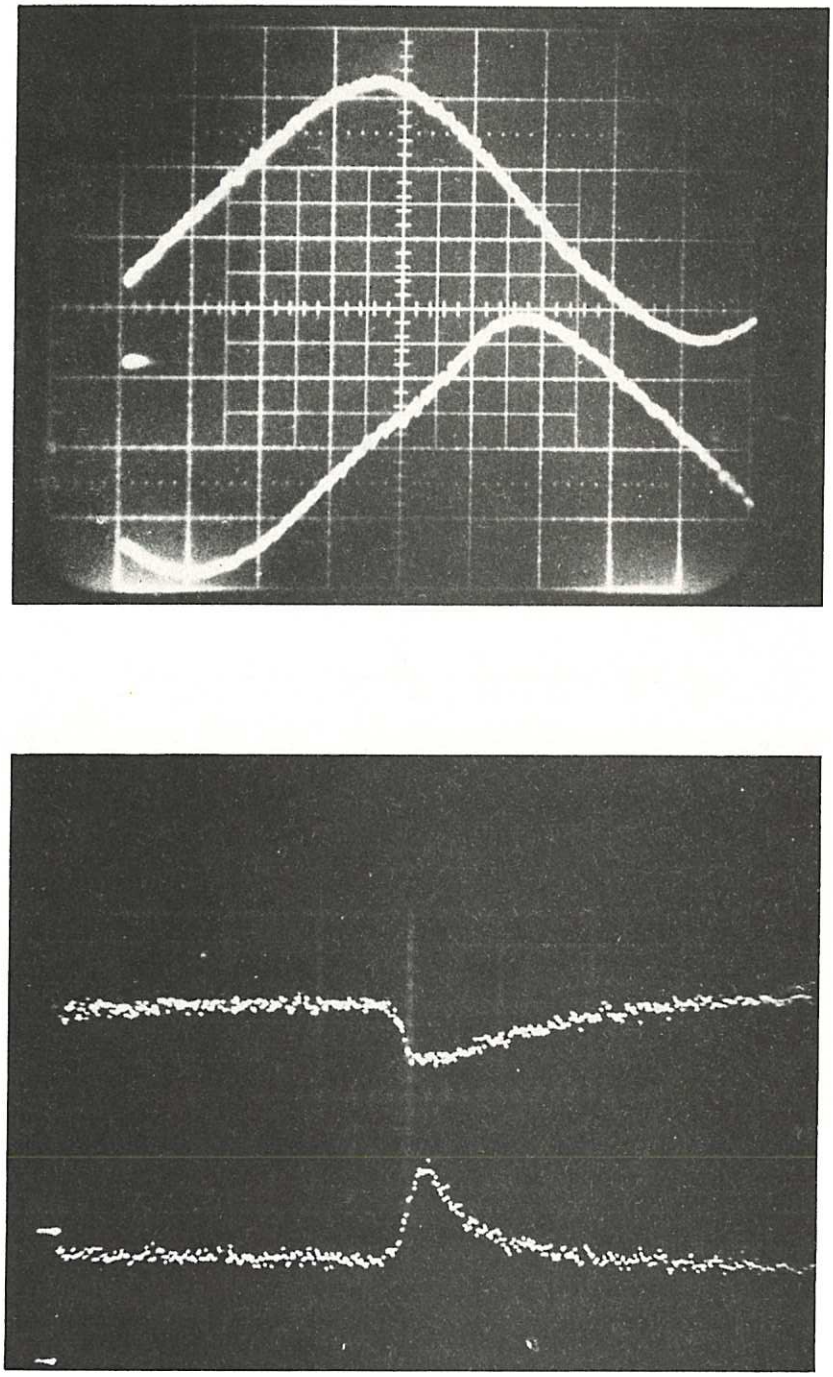

Fig.9 Quadrature waveforms cos ($\varphi_{pl} + \varphi_{vib}$) and sin ($\varphi_{pl} + \varphi_{vib}$) for 10.6$\mu$m interferometers. From Gowers and Lamb (1982).

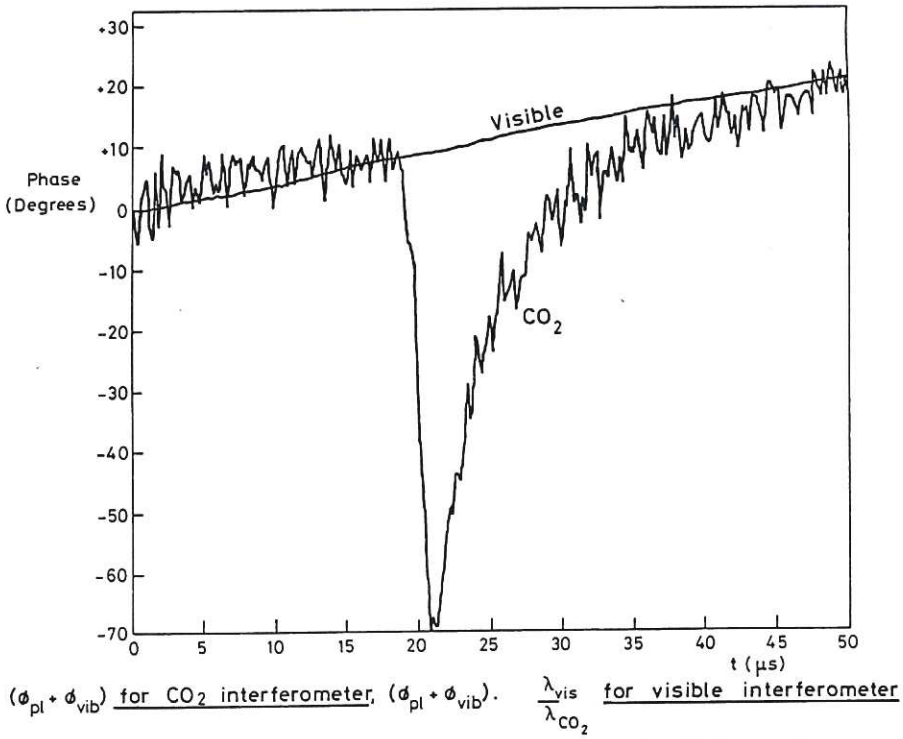

Fig.10a Total phase change ($\varphi_{pl} + \varphi_{vib}$) in degrees for 10.6 μm and 0.63/10.6 ($\varphi_{pl} + \varphi_{vib}$) for 0.63$\mu$m. Gowers and Lamb (1982).

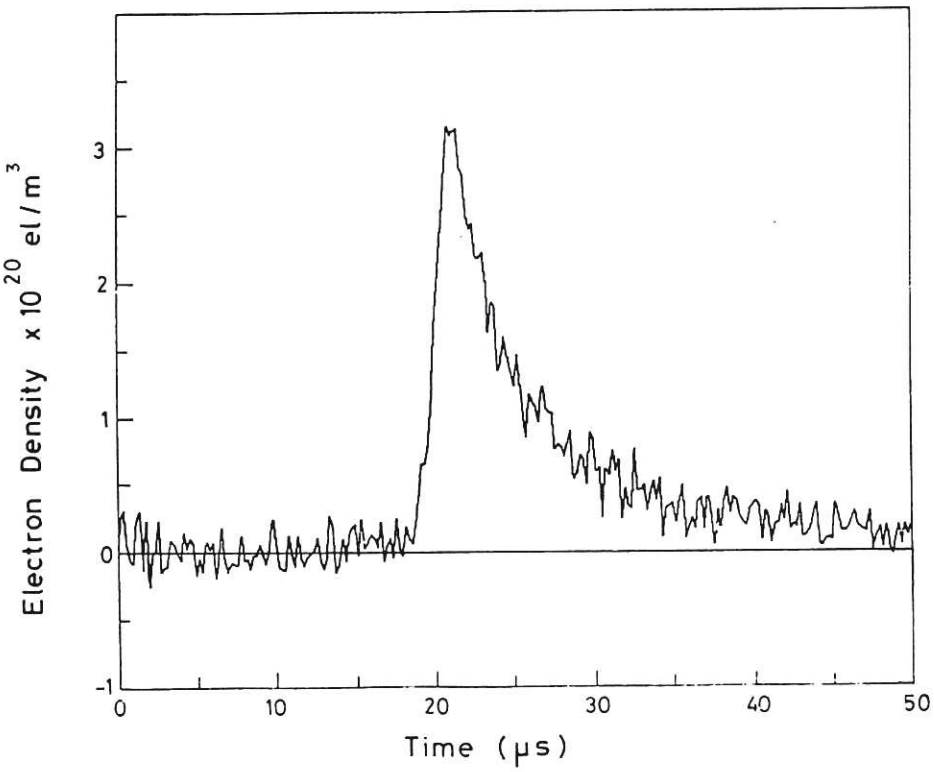

Fig.10b Phase change due to plasma alone given by the difference between the phase changes above. The result is converted to line electron density $\bar{n}_e = \frac{1}{L} \int n_e(x)\, dx$.

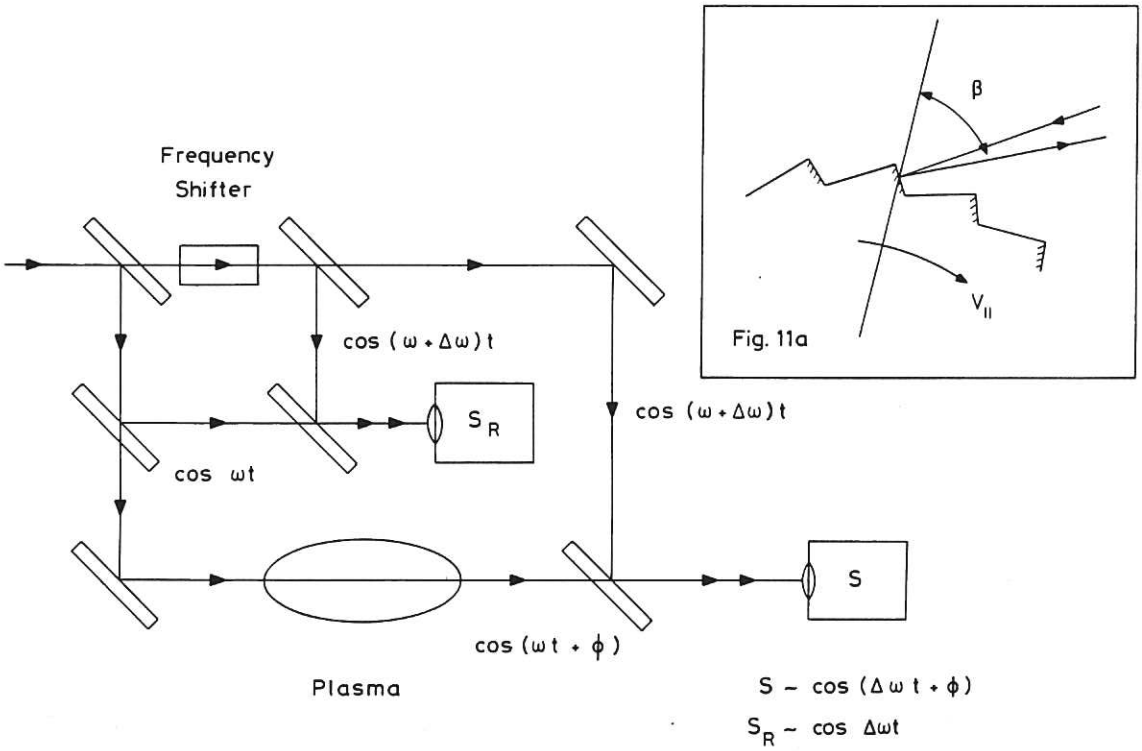

Fig.11 Schematic of phase comparison double interferometer. Main interferometer signal S is compared in phase with reference signal S_R.
Fig.11a Frequency shifter in the Veron (1974) version is a rotating cylindrical grating giving shift $\Delta\omega = (4\pi/\lambda)\, v \sin\beta$.

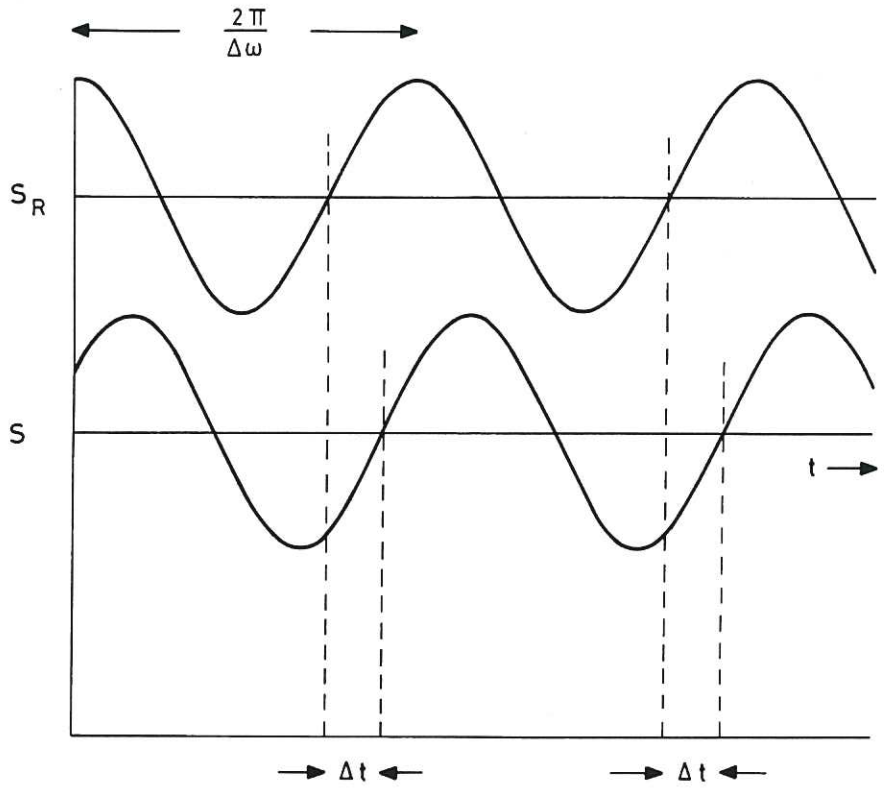

Fig.12 Analysis of the phase comparison interferometer signals $S \sim \cos(\Delta\omega t + \varphi)$ and $S_R \sim \cos \Delta\omega t$ where $\Delta\omega$ is the frequency shift.
Time elapsed between a positive slope zero crossing of S_R and the next positive slope zero crossing of S is Δt. The plasma-induced phase shift $\varphi = \Delta t\, \Delta\omega$. After Veron (1979).

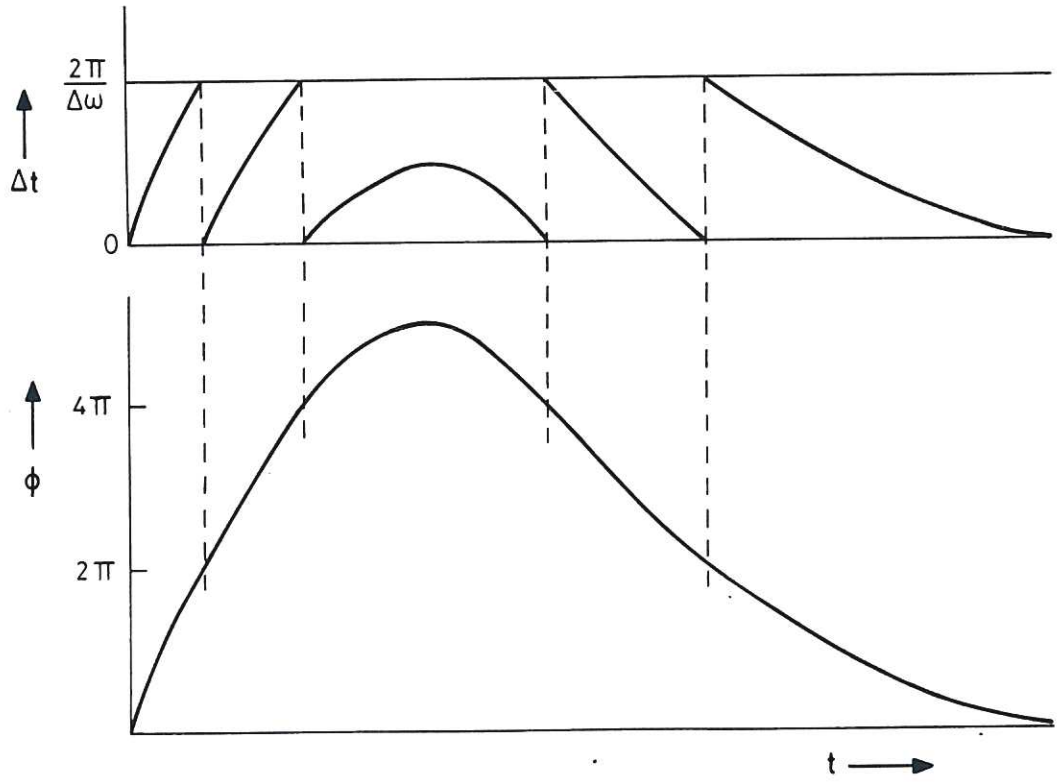

Fig.13 Display from phase comparison interferometer. Lower curve shows actual phase shift $\varphi(t)$ and upper, the interferometer display. After Magyar (1981).

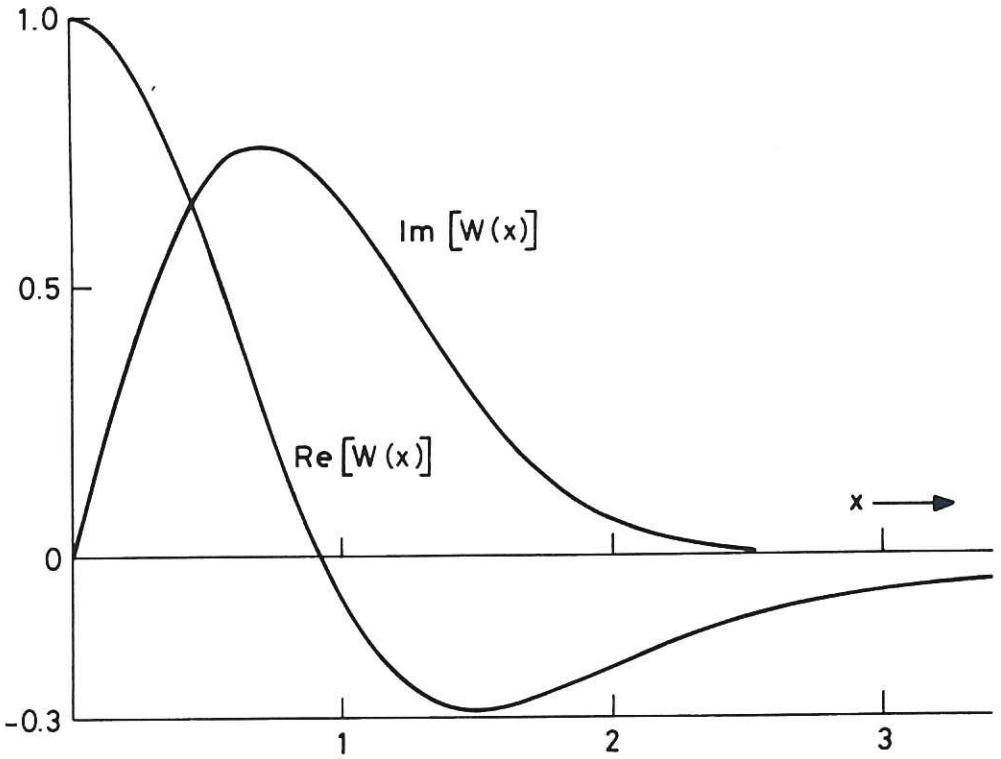

Fig.14 The real and imaginary parts of the plasma dispersion function W(x).

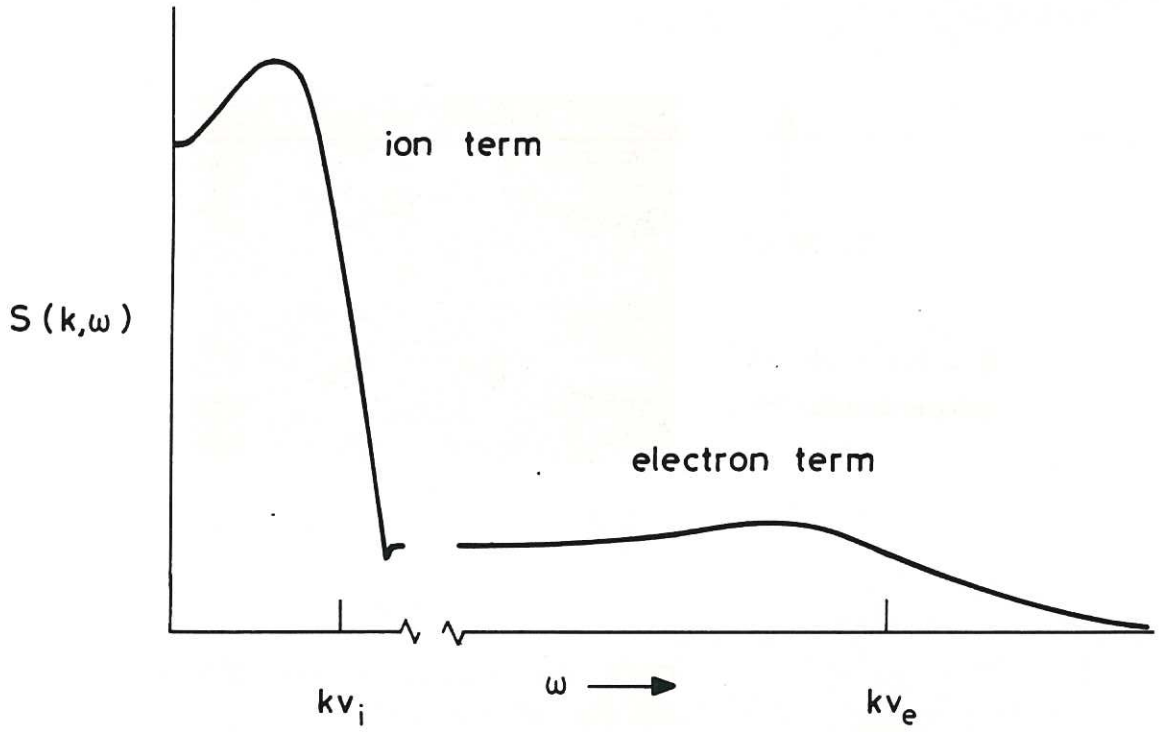

Fig.15 Frequency spectrum of scattered radiation from a thermal plasma.

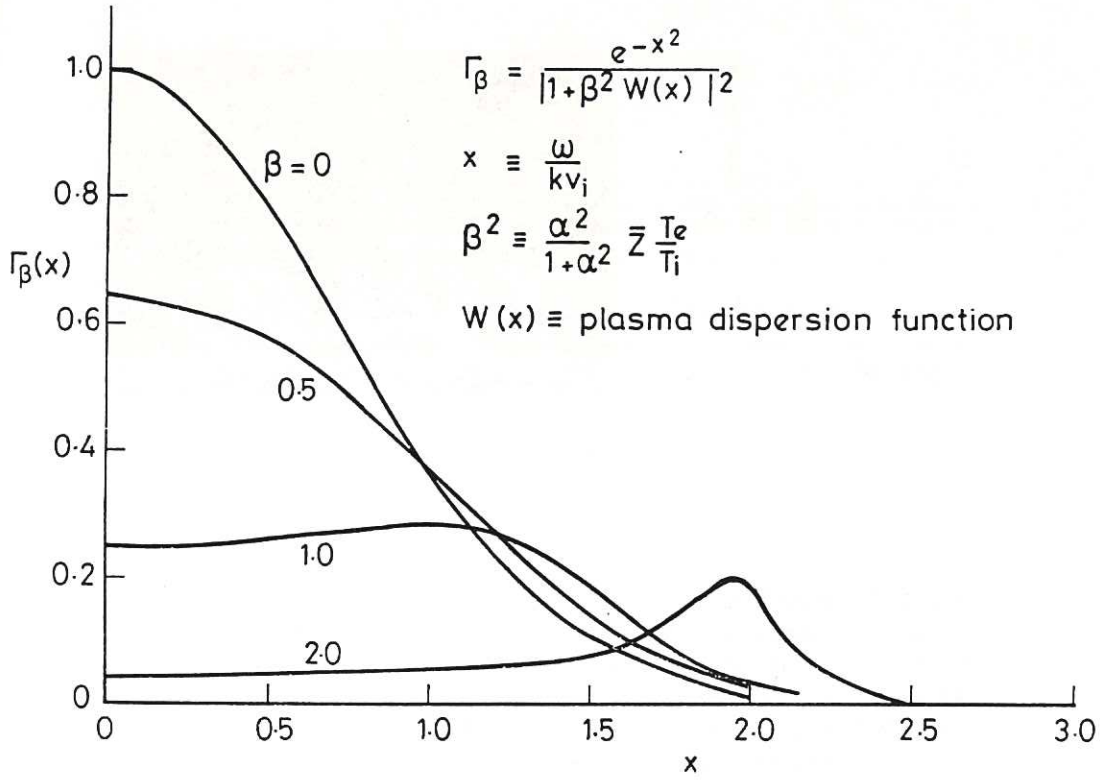

Fig.16 Collective scattering ion term illustrating its dependence on α and temperature ratio T_e/T_i.

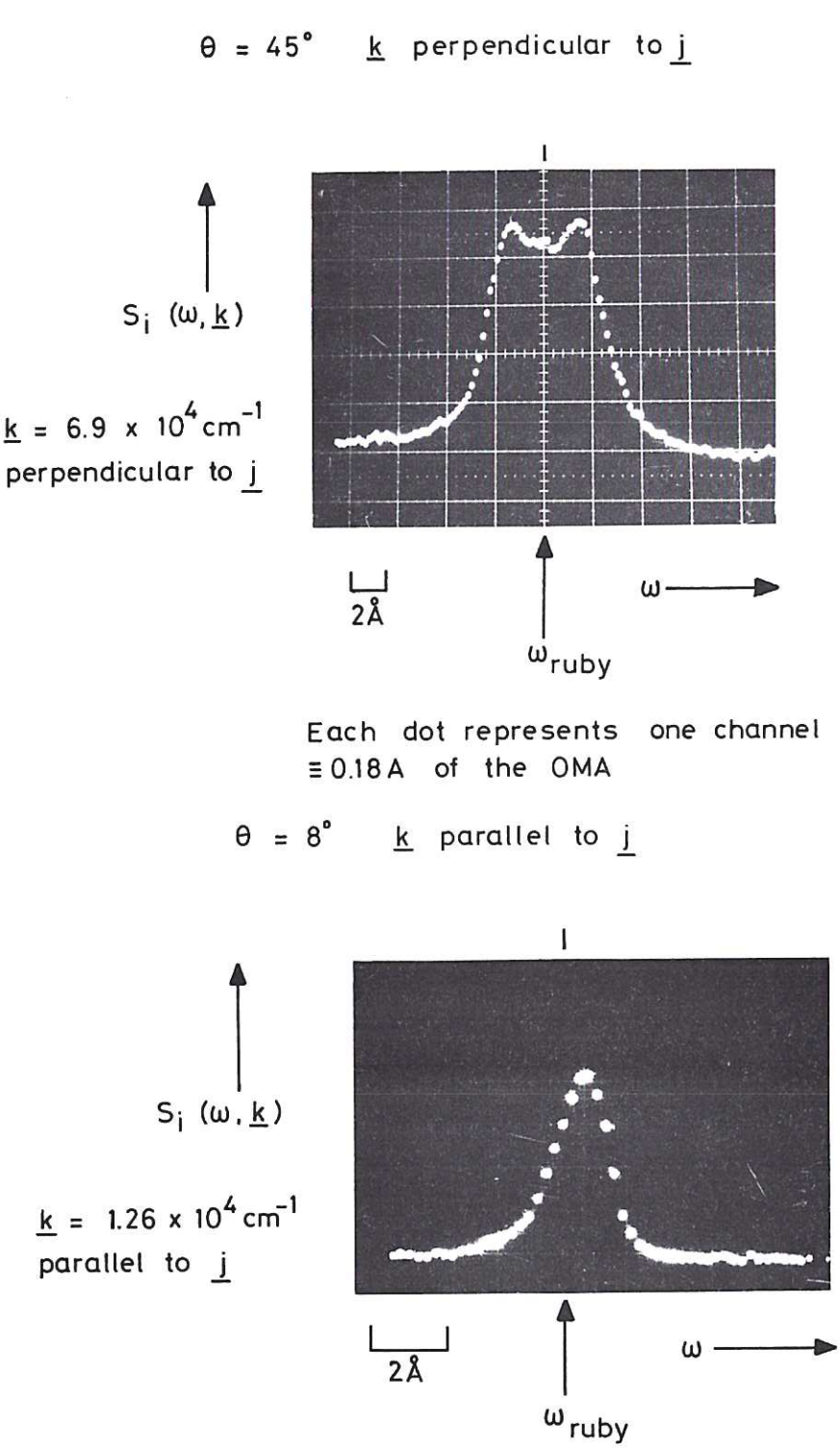

Fig.17 Single discharge ion features measured in the Culham plasma focus with a pulsed ruby laser and a multi-channel gated optical analyser (OMA).
UPPER: scattering vector k parallel to plasma current J. Scattering angle $\theta = 8°$. About 30x thermal intensity. Scale is 1 Angstrom unit per division.
LOWER: k perpendicular to J. $\theta = 45°$. Intensity approximately thermal. Scale is 2.4 Angstrom units per division. After Kirk (1982).

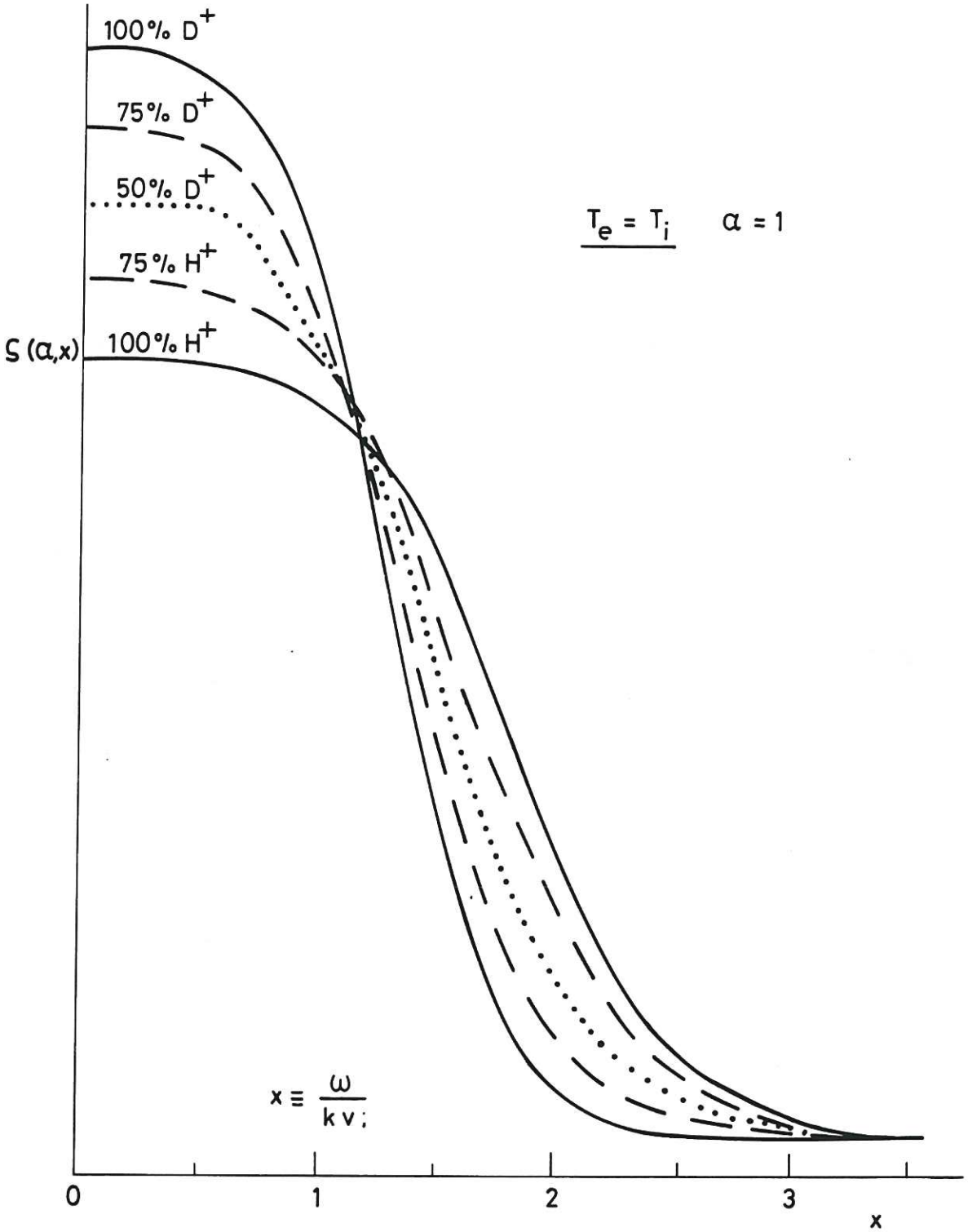

Fig.18 Ion features for plasmas composed of hydrogen plus deuterium. Relative abundance of two components varies as shown. After Stamatakis (1981).

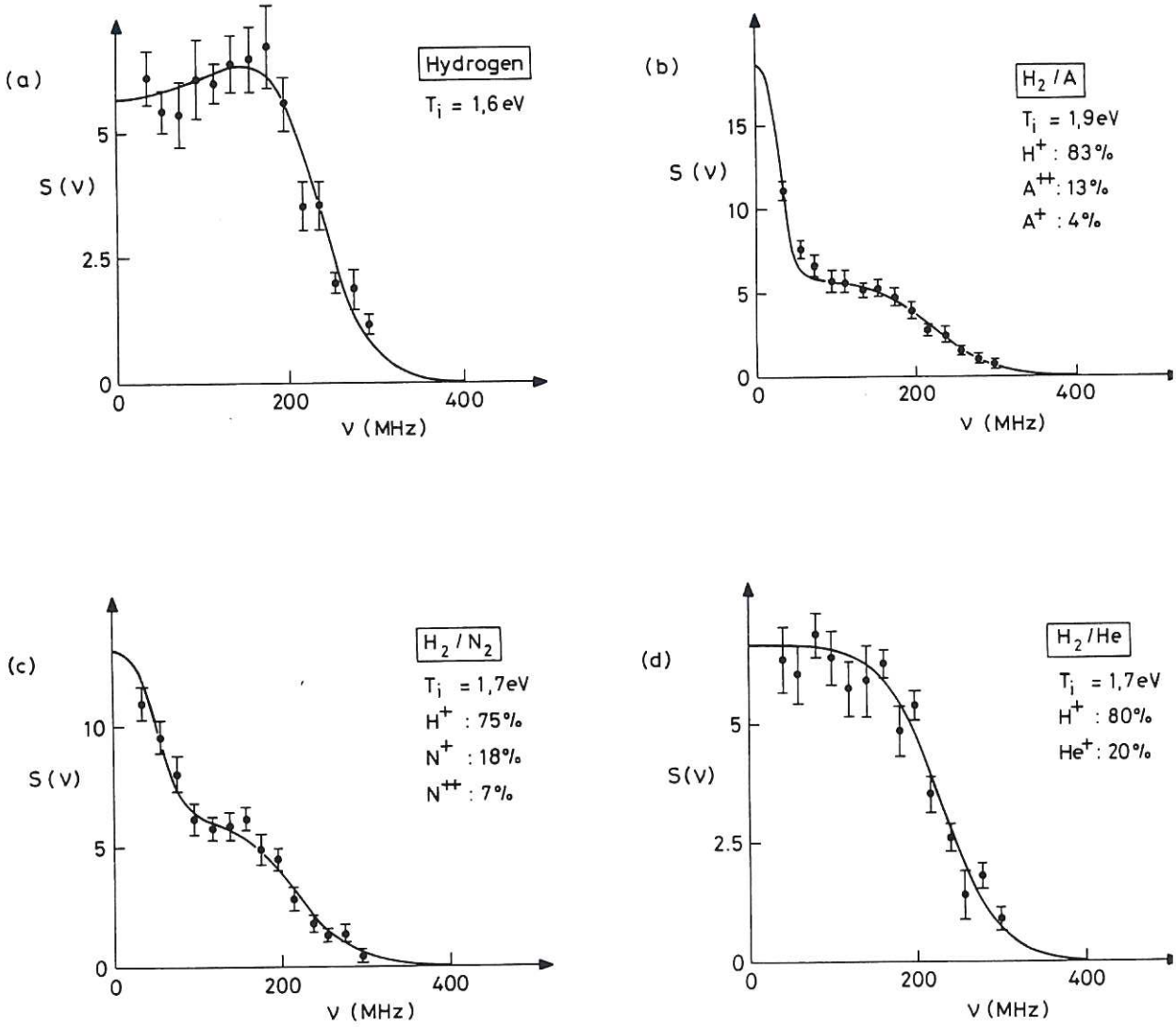

Fig.19 Spectra of composite plasmas after Kasparek and Holzhauer (1981).
(a) hydrogen alone, (b) hydrogen plus argon,
(c) hydrogen plus nitrogen, (d) hydrogen plus helium.

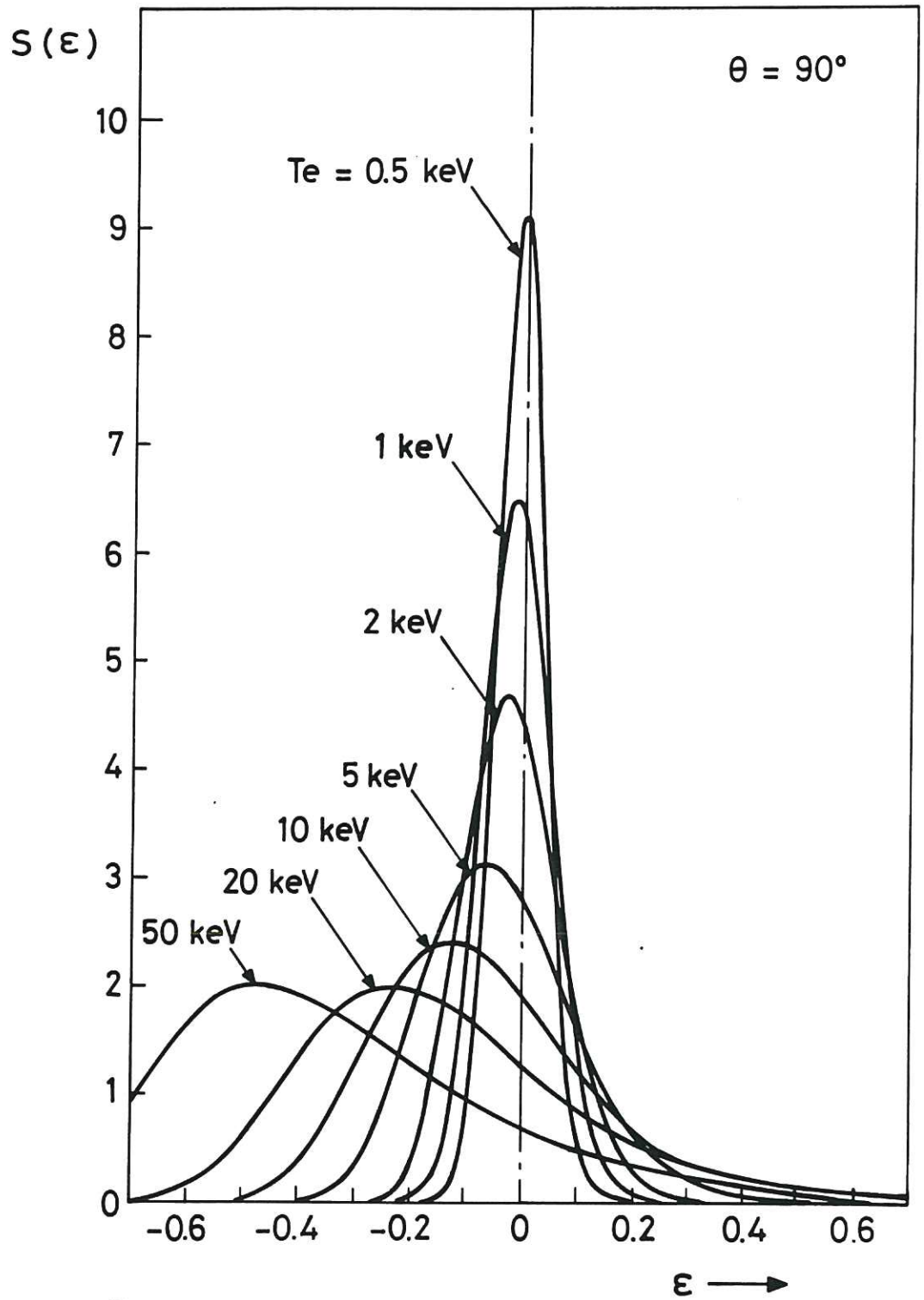

Fig.20 Spectrum of radiation incoherently scattered by relativistic plasmas. After Selden (1982).